This is a peer-reviewed, accepted author manuscript of the following research article: Buerkle, M, Padmanaban, DB, McGlynn, R, Mariotti, D & Svrcek, V 2024, 'Unexpected electronic features of NiO quantum dots produced by femtosecond pulsed laser ablation in water', Journal of Physical Chemistry Letters, vol. 15, no. 15, pp. 4185-4190. https://doi.org/10.1021/acs.jpclett.4c00458

Unexpected Electronic Features of NiO Quantum Dots produced by fs Pulsed Laser Ablation in Water

Marius Buerkle,*,† Dilli babu Padmanaban,‡ Ruairi McGlynn,‡ Davide Mariotti,‡ and Vladimir Svrcek*,†

†*National Institute of Advanced Industrial Science and Technology (AIST), Tsukuba, Ibaraki, 305-8568, Japan*
‡*School of Engineering, Ulster University, BT15 1AP, United Kingdom*

E-mail: marius.buerkle@aist.go.jp; vladimir.svrcek@aist.go.jp

Abstract

This study examines quantum confinement and surface orientations on NiO quantum dots' electronic properties. It compares NiO nanocrystals produced via atmospheric pressure microplasma and femtosecond (fs) laser ablation in water, finding both methods yield quantum-confined nanocrystals with a defined face-centered cubic lattice. Notably, fs-laser synthesis generates crystalline nanocrystals from both crystalline and amorphous targets. While the electronic properties, i.e. energy of the highest occupied molecular orbital (HOMO) and lowest unoccupied molecular orbital (LUMO), of microplasma-synthesized NiO nanocrystals are consistent with existing literature, the electronic characteristics of NiO nanocrystals produced by fs-laser, particularly the high lying LUMO level, are unusual for NiO quantum dots. Supported by density functional theory calculations, we show that the observed level positions are related to the different polar and nonpolar faces of the nanocrystal surface. Bulk Nickel oxide (NiO) is a Mott-insulator with an antiferromagnetic ordering[1] and for many applications can act as a p-type semiconductor. For example NiO thin-films are used as hole-transport layer in perovskite photovoltaic cells[2,3] or as catalytic surfaces to break down nitrite and nitric oxide[4], oxidation of carbon-monoxide[5] or photocatalytic reactions[6,7]. However, for many applications its wide-bandgap or the energy level alignment in general poses a significant challenge as it limits the efficiency of e.g. light absorption and emission or reactivity. Dimensionality reduction, going from 3D bulk NiO to 0D quantum-dots, i.e. NiO nanocrystals in the quantum-confinement regime[8,9], provides means to tailor the bandgap and electronic structure and thus control the energy range relevant for light absorption and emission and to enhance catalytic properties[9,10]. Additionally, it largely increases the surface-to-volume ratio which benefits catalytic reactions that are facilitated at the catalyst surface.

It is well-known that the crystallographic orientation of the NiO surface strongly influences the Fermi energy and surface potential[6,11]. Hence, controlling the dominant type of surface orientation of the NiO nanocrystals is essential for all possible applications.

Different synthesis methods can contribute to modify these characteristics and allow modulating surface energies associated with these orientations[12], an aspect of particular significance for nanocrystals characterized by quantum confinement sizes, i.e. smaller than the NiO exciton Bohr radius of 7.7 nm[7].

Plasma technologies provide an effective way to synthesize nanocrystals over a wide range of sizes[13,14]. The utilization of microplasma discharge has proven to be a viable method for localized and precise synthesis, yielding NiO nanocrystals characterized by quantum confinement sizes, a well-defined size distribution, and specific attributes in terms of shape and composition[15]. An alternative synthesis route is represented by short-pulsed (ns, fs) laser-induced plasma processes in liquid media[16,17]. The size of NiO nanocrystals can be readily manipulated by adjusting synthesis parameters such as laser fluence and pulse duration[18,19]. Using fs pulse laser ablation in water allows for an environmentally friendly and cost-efficient production of nanocrystals as it eliminates the need for stabilizing agents or surfactants, resulting in cleaner and purer NiO surfaces[20].

In this study, we explore and compare how plasma-based synthesis alters the electronic structure of NiO nanocrystals, particularly the energy alignment of the frontier orbitals, i.e. the highest occupied molecular orbital (HOMO) and lowest unoccupied molecular orbital (LUMO). We compare the electronic characteristics of NiO nanocrystals produced through two methods: atmospheric pressure microplasma and fs pulsed laser-induced plasma ablation in water. Both methods yield crystalline NiO nanocrystals with a well-defined face-centered cubic lattice (Fm-3m) with sizes in the quantum confinement regime. Notably, in the case of fs-laser synthesis, the phase of the target did not exert influence. While the optoelectronic characteristics of NiO nanocrystals produced by microplasma are in accordance with commonly reported results in the literature[15,21–24] the electronic features observed for NiO nanocrystals synthesized by fs-laser are peculiar as we find a much larger bandgap due to the high lying LUMO levels. First-principles calculations suggest that the difference of the electronic properties observed for NiO obtained by the two different synthesis methods can be traced back to different dominant surface orientations, which in turn strongly influences the electronic properties.

Microplasma synthesis. Low-resolution transmission electron microscope (TEM) image (Fig. 1a) confirms the presence of NiO nanocrystals synthesized by the microplasma technique. In the corresponding high-resolution TEM image (Fig. 1b) we can observe individual NiO nanocrystals and well-defined lattice fringes confirming the crystalline phase of NiO quantum dots. The fringe patterns in the high-resolution TEM images allow us to directly identify distinct lattice spacing values of 0.21 nm and 0.24 nm. These values correspond to the lattice planes associated with the (200) and (111) planes of the NiO cubic phase with values of 0.209 nm and 0.242 nm (Fig. 1c) according to JCPDS file number #780429. Overall, the TEM analysis highlights the presence of a well-defined crystal structure of the NiO nanocrystals with diameters ranging from 1.5 nm to 5.0 nm and a mean of 3.28 nm (Fig. 1d), which is well within the quantum confinement regime[8].

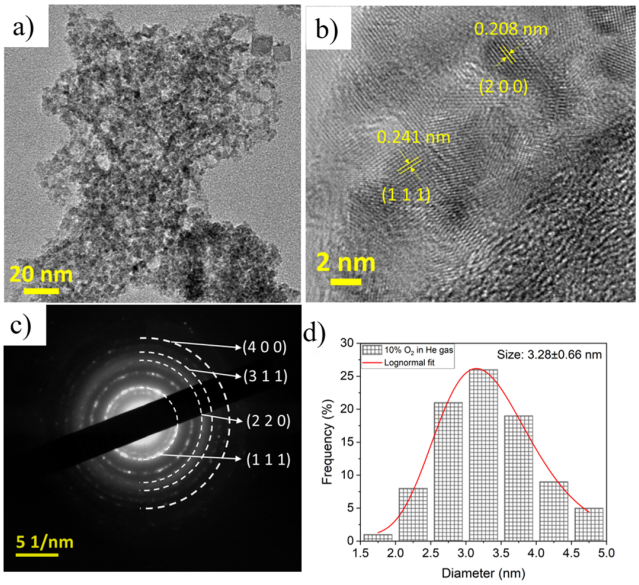

Figure 1: (a) Representative transmission electron microscopy (TEM) micrograph of NiO particles synthesized by microplasmas. (b) High-resolution TEM image showing lattice fringes of the quantum dots. (c) SAED pattern. (d) Size distribution of the NiO crystals.

fs-laser ablation. For the fs-laser ablation-based synthesis in water we use two different types of targets, namely crystalline Ni and

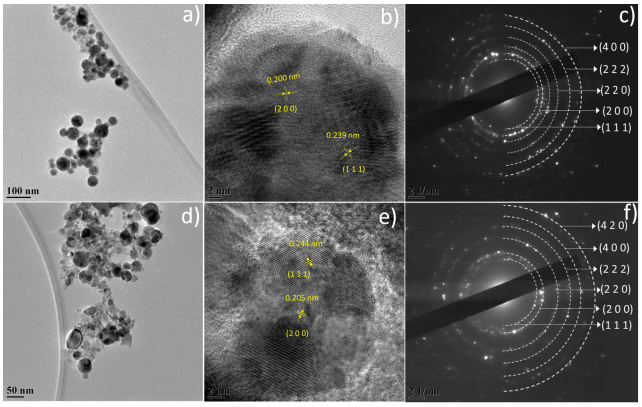

Figure 2: Results for crystalline Ni targets are given in (a)-(c) and for amorphous Ni targets (d)-(f). (a, d) Representative TEM micrograph of NiO particles produced by fs laser (Ni metallic target). (b, e) high-resolution TEM image with lattice fringes of NiO quantum dots. (c, d) TEM diffraction SEAD pattern.

amorphous NiO. In both cases TEM and SEAD confirm a well-defined NiO cubic lattice of the produced nanocrystals (Fig. 2) irrespective of the target used. To note that while large agglomerates ($>$ 25 nm, Fig. 2a and 2d) are observed, these are formed by much smaller nanocrystals (Fig. 2b and 2e), which exhibit mean diameters of approximately 4 nm (see Fig. S1 in the SI), regardless of the target used. The crystallinity and sizes of individual nanocrystals produced by fs-laser are comparable to the results obtained by microplasma synthesis, however agglomeration is one distinctive feature of the NiO nanocrystals produced by fs-laser ablation[17].

A closer analysis of the TEM images (Fig. 2b and 2e) and SEAD patterns (Fig. 2c and 2f) suggests a wide range of possible lattice planes such as (1 1 1), (2 0 0), (2 2 0), (2 2 2), and (4 0 0). In the case of the amorphous target (Fig. 2f), an additional plane, (4 2 0), was identified.

Electronic properties. In general, the optical transitions of metal oxides are tied to various energy states within the material, primarily determined by the near-band edge between HOMO and LUMO levels. For p-type metal oxide semiconductors, additional transitions correspond to energy states introduced by intraband defects, such as metal deficiency or an excess of oxygen. NiO films exhibit a reduced bandgap when prepared at the highest oxygen flow ratio, attributed to Ni vacancies or interstitial oxygen atoms[25]. Figure 3 summarizes the measured values of HOMO/LUMO levels, of the synthesized NiO nanocrystals as well as the values related to NiO bulk. The literature values for the bandgap of bulk NiO, and accordingly the VBA and CBM, vary between experiments and typically fall within the range of 2.3-3.6 eV[9].

The valence band maximum (VBM), or to be precises HOMO level, was determined by means of XPS (Figs. S2, S3). The Fermi level (EF) was established through Kelvin probe measurements (Figs. S7, S8), and the bandgap (Eg) was obtained from ultraviolet-visible (UV-VIS) transmittance using Tauc plot (Fig. S4, S5, S6). The conduction band minimum (CBM), representing the LUMO level, was determined from the VBM measurements adding the bandgap E_g.

Both, NiO nanocrystal samples synthesized by fs-laser exhibit a large bandgap above 5.4 eV. Upon comparing these results with those of the NiO nanocrystals synthesized by microplasma (Fig. 3a), a large difference in the bandgap value is observed, the latter exhibiting a bandgap of only $\approx$ 3.7 eV. This clearly underscores significant variations in the electronic properties of NiO nanocrystals depending on the employed synthesis method. While the HOMO levels, irrespective of the synthesis methods lie within the negative range 6.70 eV to 6.75 eV, the LUMO values for both samples produced by fs-laser exhibit an upward shift to -1.23 eV and -1.30 eV with respect to the microplasma-produced NiO nanocrystals, which show a value of -3.02 eV. Figure 3 also includes the level energies obtained from first-principles calculations of NiO nanocrystals, which will be discussed in the following in more detail.

Computational results. To rationalize the observed dependence of LUMO energies on the synthesis conditions, we conducted first-principles calculations of the electronic struc-

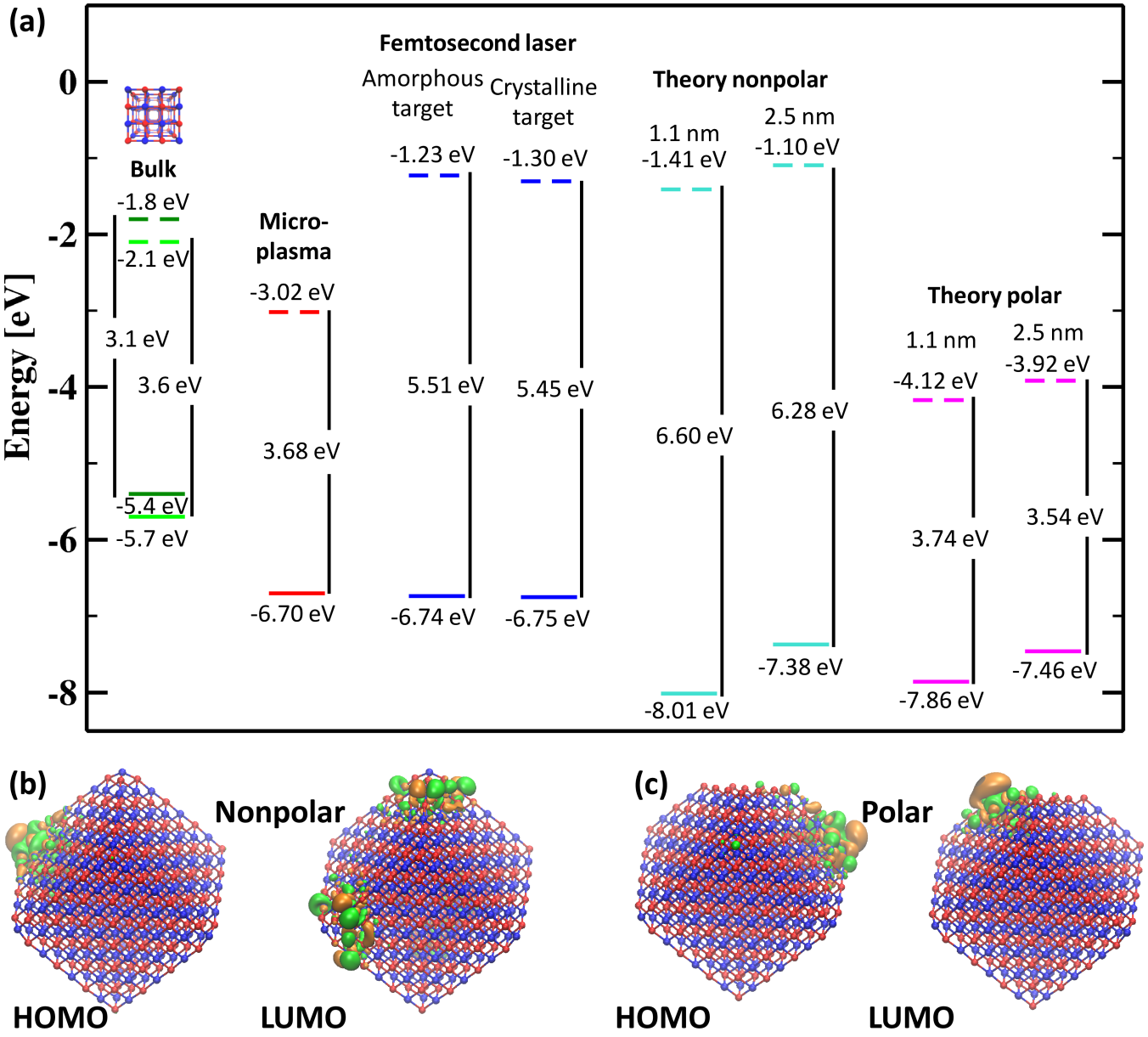

Figure 3: (a) The energy band diagram of the HOMO and LUMO levels of NiO QDs. As reference the CBM and VBM of bulk NiO bulk are include. The bulk values of the CBM and the VBM are known to vary between different measurements[9], which his indicted by the multiple values given in the diagram. The band diagrams are compared to first-principles calculations of NiO nanocrystals with a diameter of 1.1 nm and 2.5 nm with nonpolar (001) and polar (111) surfaces. HOMO and LUMO wavefunctions of the NiO nanocrystals (d = 2.5 nm) with (b) nonpolar and (c) polar surfaces. Here orange (green) indicates the isosurface of the wavefunction with positive (negative) sign.

ture of NiO particles. We considered nanocrystals with a diameter of $d = 1.1\,\mathrm{nm}$ and $d = 2.5\,\mathrm{nm}$, with either nonpolar surfaces, (100) equivalent (Fig. 3b), or with a polar (111) surface (Fig. 3c). It is known that NiO surfaces of thin films with different lattice orientations can have quite different Fermi energies and bandgaps[7,11]. We find that the HOMO position is only weakly affected by the nanocrystal's crystal surface orientation, while the LUMO shows a strong dependency on the surface orientation. This is also reflected in the wavefunctions, which is similar for the HOMO wavefunction for both non-polar and polar nanocrystals (Fig. 3b-c), while the LUMO wavefunction is delocalized over the nanocrystals for the nonpolar nanocrystal (Fig. 3b) but localized at the polar surfaces of the polar nanocrystals (Fig. 3c). This does not only hold for the HOMO and LUMO shown here but also for the next several lower (higher) occupied (unoccupied) frontier orbitals (Fig. S9). The LUMO energy of the polar nanocrystals is drastically reduced compared to the non-polar nanocrystals, accordingly, the corresponding HOMO-LUMO gap of the polar nanocrystals is also much smaller than that of the non-polar ones. The computational results show correlation of the HOMO and LUMO energies between NiO nanocrystals synthesized using fs-laser ablation and non-polar simulated NiO nanocrystals. Similarly, the HOMO and LUMO energies of the polar nanocrystals correlate with the level energies measured for the microplasma-synthesized nanocrystals, suggesting that the different synthesis methods tend to stabilize different surfaces.

Comparison micro-plasma vs fs-laser ablation. Two synthesis methods tend to favor the stabilization of distinct surfaces, resulting in either polar or nonpolar nanocrystals. NiO produced through microplasma synthesis exhibits well-separated nanocrystals. The examination of agglomeration or non-agglomeration serves as a crucial method for substantiating the inherent characteristics of surfaces synthesized through microplasma and laser techniques. This comparative analysis specifically aims to affirm the polar attributes of microplasma-synthesized surfaces and, conversely, the non-polar characteristics associated with laser-synthesized surfaces. In the context of nanocrystal synthesis via laser ablation in water, a noteworthy observation emerges. It is evident that the nanocrystals generated through this process tend to exhibit a predisposition toward assuming a non-polar nature. Consequently, this inclination leads to the aggregation or agglomeration of these nanocrystals. Thus, our experimental results corroborate the formation of distinctive surfaces with respect to the synthesis method utilized. Nonpolar nanocrystals pose a distinct challenge to the well-established Derjaguin, Landau, Verwey, and Overbeek theory[26–28]. This challenge stems from the theory's incapacity to explain the colloidal stability of non-polar nanocrystals, primarily due to the absence of charge stabilization. More precisely, van der Waals forces come into play, drawing NiO nanocrystals towards each other. However, electrostatic forces, encompassing the repulsion between charged particles, counteract this attraction, preventing the nanocrystals from coming too close. This phenomenon provides a rationale for the observed agglomeration in polar (111) and nonpolar ((200), (220), (400), and (420)) nanocrystal surfaces synthesized through laser-based methods. Intriguingly, these agglomerated structures, by the end of the process, exhibit nonpolar properties due to the excess of nonpolar surfaces within the agglomerates (Fig. 2c and Fig. 2f). In contrast, the non-agglomeration observed in polar nanocrystals synthesized through microplasma-based methods remains distinctive in its behavior. play, drawing NiO nanocrystals towards each other. However, electrostatic forces, encompassing the repulsion between charged particles, counteract this attraction, preventing the nanocrystals from coming too close. This phenomenon provides a rationale for the observed agglomeration in polar (111) and nonpolar ((200), (220), (400), and (420)) nanocrystal surfaces synthesized through laser-based methods. Intriguingly, these agglomerated structures, by the end of the process, exhibit nonpolar properties due to the excess of nonpolar surfaces within the

agglomerates (Fig. 2c and Fig. 2f). In contrast, the non-agglomeration observed in polar nanocrystals synthesized through microplasma-based methods remains distinctive in its behavior. During the cooling step of the fs-laser synthesized NiO nanocrystals are ejected into water and tend to form relatively small agglomerates (d = 25 nm).

In summary, by employing two distinct synthesis methods, we compared the properties of resulting NiO nanocrystals. Each technique yielded different nanocrystal configurations, influencing the electronic structure and energy levels. Our focus centered on exploring the positions of the HOMO and LUMO levels in NiO nanocrystals, considering the impact of quantum confinement and a strong dependency on the surface orientation. Synthesis by fs-laser synthesis produced unexpected results, revealing that a peculiar NiO nanocrystal surface orientation induced significant changes in the LUMO levels. For this, we employed computationally intensive hybrid density functional theory calculations at the CAM-B3LYP level to precisely characterize electronic structure. This comparative analysis using different synthesis techniques enhances our understanding of how synthesis parameters and nanocrystal properties influence electronic structure. Experimental data agree well with DFT calculations. This study contributes to a comprehensive understanding of the electronic properties of NiO nanocrystals, a crucial aspect for customizing applications.

Methods

Synthesis by microplasmas. The synthesis of the NiO nanocrystals has followed a methodology previously used for the synthesis of a range of other metal and metal oxide nanoparticles[29–33]. Briefly, the synthesis setup consists of a microplasma reactor with two ceramic tubes placed coaxially in which the inner tube (O.D.-1.3 mm, I.D.-0.7mm) contains a 0.5 mm diameter nickel wire (99.99% purity, purchased from Alfa Aesar) whereas the outer ceramic tube (O.D.-3mm, I.D.-2mm) hosts precursor gases. Both tubes pass through double copper electrode which is powered by a radio frequency (13.56 MHz) power supply. Both wire and ceramic tubes were placed through a "T" shaped metal Swagelok fitting where gas inlets also connected. Whereas the other end of the wire and inner ceramic capillary are placed in such a way that the wire is exposed to the precursor gas placed inside the two electrodes. All these components were placed in support through a perspex frame. The deposition process is performed for different oxygen concentrations with constant 500 sccm He gas flow, 56 sccm oxygen gas (10 % oxygen gas fraction) flow and 70 W RF power. The entire process was carried out for a duration of 2 minutes and characterized using different techniques. These films were used to study the material properties.

Synthesis by fs-laser in water. NiO nanocrystal agglomerates are fabricated by femtosecond laser (Libra Solo Ultrafast Optical Parametric Amplifier-OPerA) ablation in deionized (DI) water of a 5 mm thick metallic Ni and/or amorphous NiO target. The target is immersed in 6 mL of high purity DI water with a resistivity of about 15 MΩ The power is about 500 mW, with a pulse of 83 fs at 1 kHz frequency, and a wavelength of 400 nm for 1 h of irradiation. The laser beam was shaped and focused onto a spot on the target surface by an optical lens with a focal length of 250 mm. The focal point area of the laser beam on the target is estimated to be approximately 1 mm2. The target is rotated for better homogeneity and to avoid irradiating the exact same spot for the next pulse.

Transmission electron microscopy (TEM). The crystal structure and morphology of the NiO nanocrystals were elucidated using TEM (JOEL, JEM-2100F), Gatan DualVision 600 Charge-Coupled Device (CCD) at accelerating voltage of 200 kV. For TEM, samples were prepared by depositing 40 µL of the nanocrystal colloidal solution in ethanol onto a holey carbon-coated grid (400 mesh, #S187-4, Agar Scientific) with an ultrathin carbon film (3 nm thick) and allowed to evaporate under ambient conditions overnight. The d-spacing values of the crystal planes were measured on the digital image using ImageJ software. The sam-

ples were prepared initially by depositing the nanocrystals onto a n-type Si substrate, then scratched, redispersed as a colloid in ethanol (purity 99.8%, Sigma Aldrich).

First-principles modeling. Bulk nickel oxide is a Mott-insulator with an antiferromagnetic ground state[1], that is very difficult to accurately describe using local (semi-local) density functional theory (DFT). While DFT+U gives reasonably accurate results for bulk NiO[34,35] it is doubtful that surface and finite size effects present in nanocrystals are accurately captured. Therefore, we employ here, while for the studied particle size computationally very expansive, hybrid density functional theory calculations at the CAM-B3LYP level of theory[36] to accurately describe the electronic structure of the nanocrystals. The results are obtained for a fairly large basis set of def2-TZVP quality[37], a comparison with the smaller def2-SV(P) basis set can be found in the supporting information (Fig. S10). Additionally we provide a short comparison of orbital energies obtained with a semi-local functional (PBE[38,39]), screened hybrid functional (HSE06[40–42]), and a global hybrid functional (PBE0[43,44]).

Using the surface energies for the different surface orientations[12] we estimate the energetically most favorable structure from a Wulff construction which is essentially terminated by nonpolar surfaces symmetry equivalent to (100) which is observed to be the natural cleavage plane[5]. Additionally, we consider capped nanocrystals which model the experimentally observed possibility of cut planes resulting in polar (111) surfaces[7,27]. All structures are relaxed using neural network potentials[45], before obtaining the electronic structure at the CAM-B3LYP level of theory.

Supporting Information Available

Experimental material characterization and properties measurements.
Band energy diagrams and Kelvin probe measurements.
Details of the first-principles calculations.
Atomic structure coordinates.

Acknowledgement This research was supported by Kakenhi 20H02579 by the Japanese Promotion of Sciences (JSPS), Japan and by EPSRC (EP/V055232/1 and EP/R008841/1)

References

(1) Anisimov, V. I.; Korotin, M. A.; Kurmaev, E. Z. Band-structure description of Mott insulators (NiO, MnO, FeO, CoO). *J. Phys. Condens. Matter* **1990**, *2*, 3973.

(2) Singh, R.; Singh, P. K.; Bhattacharya, B.; Rhee, H.-W. Review of current progress in inorganic hole-transport materials for perovskite solar cells. *Appl. Mater. Today* **2019**, *14*, 175–200.

(3) Sajid, S.; Elseman, A. M.; Huang, H.; Ji, J.; Dou, S.; Jiang, H.; Liu, X.; Wei, D.; Cui, P.; Li, M. Breakthroughs in NiOx-HTMs towards stable, low-cost and efficient perovskite solar cells. *Nano Energy* **2018**, *51*, 408–424.

(4) Derikvand, Z.; Rahmati, F.; Azadbakht, A. Nano NiO/AlMCM-41, a green synergistic, highly efficient and recyclable catalyst for the reduction of nitrophenols. *Appl. Organomet. Chem.* **2019**, *33*, e4864, e4864 AOC-18-1137.R1.

(5) Dey, S.; Mehta, N. S. Oxidation of carbon monoxide over various nickel oxide catalysts in different conditions: A review. *Chem. Eng. J. Adv.* **2020**, *1*, 100008.

(6) Hu, C.-C.; Teng, H. Structural features of p-type semiconducting NiO as a co-catalyst for photocatalytic water splitting. *J. Catal.* **2010**, *272*, 1–8.

(7) Poulain, R.; Klein, A.; Proost, J. Electrocatalytic Properties of (100)-, (110)-, and (111)-Oriented NiO Thin Films toward the Oxygen Evolution Reaction. *J. Phys. Chem. C* **2018**, *122*, 22252–22263.

(8) Duan, W. J.; Lu, S. H.; Wu, Z. L.; Wang, Y. S. Size Effects on Properties of NiO Nanoparticles Grown in Alkalisalts. *J. Phys. Chem. C* **2012**, *116*, 26043–26051.

(9) Ezhilarasi, A. A.; Vijaya, J. J.; Kaviyarasu, K.; Maaza, M.; Ayeshamariam, A.; Kennedy, L. J. Green synthesis of NiO nanoparticles using Moringa oleifera extract and their biomedical applications: Cytotoxicity effect of nanoparticles against HT-29 cancer cells. *J. Photochem. Photobiol., B* **2016**, *164*, 352–360.

(10) Ezhilarasi, A.; Vijaya, J.; Kaviyarasu, K.; Kennedy, L.; R. Jothi, R.; A., H. Green synthesis of NiO nanoparticles using Aegle marmelos leaf extract for the evaluation of in-vitro cytotoxicity, antibacterial and photocatalytic properties. *J. Photochem. Photobiol., B* **2018**, *180*, 39–50.

(11) Leonov, I.; Biermann, S. Electronic correlations at paramagnetic (001) and (110) NiO surfaces: Charge-transfer and Mott-Hubbard-type gaps at the surface and subsurface of (110) NiO. *Phys. Rev. B* **2021**, *103*, 165108.

(12) Xiang, J.; Xiang, B.; Cui, X. NiO nanoparticle surface energy studies using first principles calculations. *New J. Chem.* **2018**, *42*, 10791–10797.

(13) Scott, J. H. J.; Majetich, S. A.; Turgut, Z.; Mchenry, M. E.; Boulos, M. Carbon Coated Nanoparticle Composites Synthesized in an RF Plasma Torch. *MRS Proc.* **1996**, *457*.

(14) Rao, N.; Girshick, S.; Heberlein, J.; McMurry, P.; Jones, S.; Hansen, D.; Micheel, B. Nanoparticle formation using a plasma expansion process. *Plasma Chem. Plasma P.* **1995**, *15*, 581–606.

(15) Chakrabarti, S.; Carolan, D.; Alessi, B.; Maguire, P.; Svrcek, V.; Mariotti, D. Microplasma-synthesized ultra-small NiO nanocrystals, a ubiquitous hole transport material. *Nanoscale Adv.* **2019**, *1*, 4915–4925.

(16) Amoruso, S.; Bruzzese, R.; Wang, X.; Nedialkov, N. N.; Atanasov, P. A. Femtosecond laser ablation of nickel in vacuum. *J. Phys. D: Appl. Phys.* **2007**, *40*, 331–340.

(17) Muñetón Arboleda, D.; Santillán, J. M. J.; Mendoza Herrera, L. J.; van Raap, M. B. F.; Mendoza Zélis, P.; Muraca, D.; Schinca, D. C.; Scaffardi, L. B. Synthesis of Ni Nanoparticles by Femtosecond Laser Ablation in Liquids: Structure and Sizing. *J. Phys. Chem. C* **2015**, *119*, 13184–13193.

(18) Jaleh, B.; Torkamany, M. J.; Golbedaghi, R.; Noroozi, M.; Habibi, S.; Samavat, F.; Hamedan, V. J.; Albeheshti, L. Preparation of Nickel Nanoparticles via Laser Ablation in Liquid and Simultaneously Spectroscopy. *Adv. Mater. Resswitz.* **2012**, *403-408*, 4440–4444.

(19) Liu, B.; Hu, Z.; Che, Y.; Chen, Y.; Pan, X. Nanoparticle generation in ultrafast pulsed laser ablation of nickel. *Appl. Phys. Lett.* **2007**, *90*, 044103.

(20) Musaev, O. R.; Yan, J.; Dusevich, V.; Wrobel, J. M.; Kruger, M. B. Ni nanoparticles fabricated by laser ablation in water. *Appl. Phys. A* **2014**, *116*, 735–739.

(21) Zhu, Z.; Bai, Y.; Zhang, T.; Liu, Z.; Long, X.; Wei, Z.; Wang, Z.; Zhang, L.; Wang, J.; Yan, F.; Yang, S. High-Performance Hole-Extraction Layer of Sol–Gel-Processed NiO Nanocrystals for Inverted Planar Perovskite Solar Cells. *Angew. Chem. Int. Ed.* **2014**, *53*, 12571–12575.

(22) Li, G.; Deng, K.; Dou, Y.; Liao, Y.; Wang, D.; Wu, J.; Lan, Z. Self-assembled NiO microspheres for efficient inverted mesoscopic perovskite solar cells. *Sol. Energy* **2019**, *193*, 111–117.

(23) Zhang, W.; Zhang, X.; Wu, T.; Sun, W.; Wu, J.; Lan, Z. Interface engineering with NiO nanocrystals for highly efficient and stable planar perovskite solar cells. *Electrochim. Acta* **2019**, *293*, 211–219.

(24) Tang, J.; Jiao, D.; Zhang, L.; Zhang, X.; Xu, X.; Yao, C.; Wu, J.; Lan, Z. High-performance inverted planar perovskite solar cells based on efficient hole-transporting layers from well-crystalline NiO nanocrystals. *Sol. Energy* **2018**, *161*, 100–108.

(25) Wang, K.-C.; Shen, P.-S.; Li, M.-H.; Chen, S.; Lin, M.-W.; Chen, P.; Guo, T.-F. Low-Temperature Sputtered Nickel Oxide Compact Thin Film as Effective Electron Blocking Layer for Mesoscopic NiO/CH3NH3PbI3 Perovskite Heterojunction Solar Cells. *ACS Appl. Mater. Interfaces* **2014**, *6*, 11851–11858.

(26) Derjaguin, B.; Landau, L. Theory of the stability of strongly charged lyophobic sols and of the adhesion of strongly charged particles in solutions of electrolytes. *Prog. Surf. Sci.* **1993**, *43*, 30–59.

(27) Goniakowski, J.; Finocchi, F.; Noguera, C. Polarity of oxide surfaces and nanostructures. *Rep. Prog. Phys.* **2007**, *71*, 016501.

(28) Boström, M.; Deniz, V.; Franks, G.; Ninham, B. Extended DLVO theory: Electrostatic and non-electrostatic forces in oxide suspensions. *Adv. Colloid Interfac.* **2006**, *123–126*, 5–15.

(29) McGlynn, R.; Brunet, P.; Chakrabarti, S.; Ganguly, A.; Moghaieb, H.; Bo, Z.; Maguire, P.; Mariotti, D. A Single-Step Process to Produce Carbon Nanotube-Zinc Compound Hybrid Materials. *Small Methods* **2023**, *8*.

(30) Jain, G.; Macias-Montero, M.; Velusamy, T.; Maguire, P.; Mariotti, D. Porous zinc oxide nanocrystalline film deposition by atmospheric pressure plasma: Fabrication and energy band estimation. *Plasma Process. Polym.* **2017**, *14*.

(31) Jain, G.; Rocks, C.; Maguire, P.; Mariotti, D. One-step synthesis of strongly confined, defect-free and hydroxy-terminated ZnO quantum dots. *Nanotechnology* **2020**, *31*, 215707.

(32) Brunet, P.; McGlynn, R. J.; Alessi, B.; Smail, F.; Boies, A.; Maguire, P.; Mariotti, D. Surfactant-free synthesis of copper nanoparticles and gas phase integration in CNT-composite materials. *Nanoscale Adv.* **2021**, *3*, 781–788.

(33) Haq, A. U.; Askari, S.; McLister, A.; Rawlinson, S.; Davis, J.; Chakrabarti, S.; Svrcek, V.; Maguire, P.; Papakonstantinou, P.; Mariotti, D. Size-dependent stability of ultra-small α-/β-phase tin nanocrystals synthesized by microplasma. *Nat. Commun.* **2019**, *10*.

(34) Anisimov, V. I.; Zaanen, J.; Andersen, O. K. Band theory and Mott insulators: Hubbard U instead of Stoner I. *Phys. Rev. B* **1991**, *44*, 943–954.

(35) Dudarev, S. L.; Botton, G. A.; Savrasov, S. Y.; Humphreys, C. J.; Sutton, A. P. Electron-energy-loss spectra and the structural stability of nickel oxide: An LSDA+U study. *Phys. Rev. B* **1998**, *57*, 1505–1509.

(36) Yanai, T.; Tew, D. P.; Handy, N. C. A new hybrid exchange–correlation functional using the Coulomb-attenuating method (CAM-B3LYP). *Chem. Phys. Lett.* **2004**, *393*, 51–57.

(37) Weigend, F.; Ahlrichs, R. Balanced basis sets of split valence, triple zeta valence and quadruple zeta valence quality for H to Rn: Design and assessment of accuracy. *Phys. Chem. Chem. Phys.* **2005**, *7*, 3297.

(38) Perdew, J. P.; Burke, K.; Ernzerhof, M. Generalized Gradient Approximation Made Simple. *Phys. Rev. Lett.* **1996**, *77*, 3865–3868.

(39) Perdew, J. P.; Burke, K.; Ernzerhof, M. Generalized Gradient Approximation Made Simple [Phys. Rev. Lett. 77, 3865 (1996)]. *Phys. Rev. Lett.* **1997**, *78*, 1396–1396.

(40) Heyd, J.; Scuseria, G. E.; Ernzerhof, M. Hybrid functionals based on a screened Coulomb potential. *J. Chem. Phys.* **2003**, *118*, 8207–8215.

(41) Heyd, J.; Scuseria, G. E.; Ernzerhof, M. Erratum: "Hybrid functionals based on a screened Coulomb potential" [J. Chem. Phys. 118, 8207 (2003)]. *J. Chem. Phys.* **2006**, *124*.

(42) Krukau, A. V.; Vydrov, O. A.; Izmaylov, A. F.; Scuseria, G. E. Influence of the exchange screening parameter on the performance of screened hybrid functionals. *J. Chem. Phys.* **2006**, *125*.

(43) Adamo, C.; Barone, V. Toward reliable density functional methods without adjustable parameters: The PBE0 model. *J. Chem. Phys.* **1999**, *110*, 6158–6170.

(44) Ernzerhof, M.; Scuseria, G. E. Assessment of the Perdew–Burke–Ernzerhof exchange-correlation functional. *J. Chem. Phys.* **1999**, *110*, 5029–5036.

(45) Deng, B.; Zhong, P.; Jun, K.; Riebesell, J.; Han, K.; Bartel, C. J.; Ceder, G. CHGNet as a pretrained universal neural network potential for charge-informed atomistic modelling. *Nat. Mach. Intell.* **2023**, 1–11.

TOC Graphic

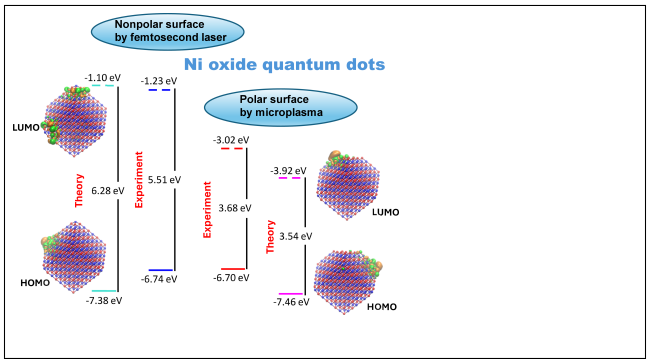
Nonpolar surface
by femtosecond laser
Ni oxide quantum dots
Polar surface
by microplasma
-1.10 eV
-1.23 eV
LUMO
Theory
6.28 eV
Experiment
5.51 eV
HOMO
-7.38 eV
-6.74 eV
-3.02 eV
-3.92 eV
Experiment
3.68 eV
Theory
3.54 eV
LUMO
-6.70 eV
-7.46 eV
HOMO

Supporting Information: Unexpected Electronic Features of NiO Quantum Dots produced by fs Pulsed Laser Ablation in Water

Marius Buerkle,*,† Dilli babu Padmanaban,‡ Ruairi McGlynn,‡ Davide Mariotti,‡ and Vladimir Svrcek*,†

†*National Institute of Advanced Industrial Science and Technology (AIST), Tsukuba, Ibaraki, 305-8568, Japan*

‡*School of Engineering, Ulster University, BT15 1AP, United Kingdom*

E-mail: marius.buerkle@aist.go.jp; vladimir.svrcek@aist.go.jp

Agglomerated NiO nanocrystals

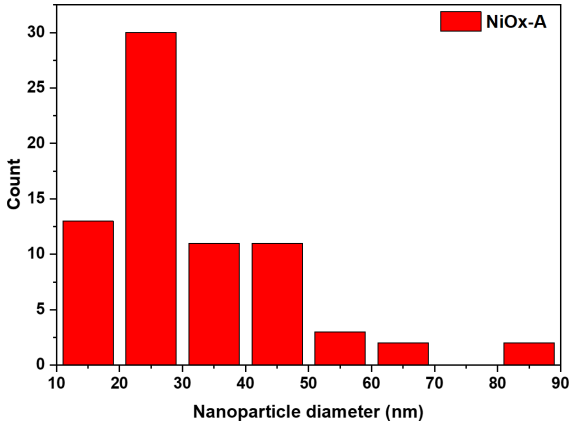

Figure S1: Typical size distribution of NiO nanocrystals agglomerates fabricated by fs laser in water.

Additional material characterization and properties measurements

X-ray photoelectron spectroscopy (XPS) was performed by direct deposition of NiO QDs on gold-coated silicon substrates. Analysis was performed using an ESCALAB Xi+ spectrometer microprobe (Thermo Fisher Scientific) with a focussed monochromatic Al Kα X-ray source ($h\nu$ = 1486.6 eV, 650 µm spot size) operating at a power of 225 W (15 kV and 15 mA) and the photoelectrons were collected using a 180° double-focusing hemispherical analyser with a dual detector system. The energy scale of spectrometer was calibrated with sputter cleaned pure reference samples Au, Ag and Cu (Au 4f7/2, Ag 3d5/2 and Cu 3p3/2) positioned at binding energies 83.96 eV, 368.21 eV and 932.62 eV, respectively. The base pressure in the analysis chamber was better than 5x10-9 mbar, which increased up to 5x10-7 mbar with charge neutraliser (flood gun) operated at 100 µA emission current. For the Fermi level alignment, a copper strip was used to make a good electrical contact between the sample and the spectrometer. For all the samples analysed, the survey spectra were recorded with a step size of 1 eV and a pass energy of 150 eV and the narrow scans were recorded with a step size of 0.1 eV and a pass energy of 20 eV. This pass energy gives a 0.65 eV width for the Ag 3d5/2 peak measured on a sputter cleaned Ag sample. The spectra obtained were

charge corrected using Au core level and valence band spectra.

The optical characteristics of the NiO nanocrystals were evaluated by forming films on quartz substrates. Measurements were taken with a Perkin Elmer-Lambda 1050+ spectrometer. The optical transmittance (T) of the films was recorded in the transmittance compartment and the corresponding absorption coefficients were estimated to produce Tauc plot in the assumption that reflectance was negligible.

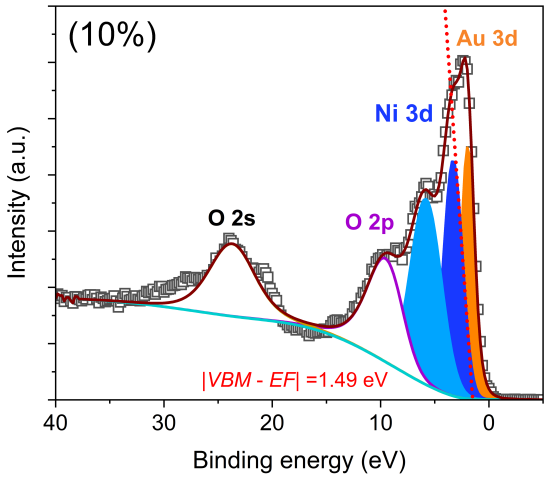

Figure S2: XPS valence band spectra of NiO produced by microplasmas show the energy difference between the energy level of the valence band maximum (VBM) and the Fermi level (EF).

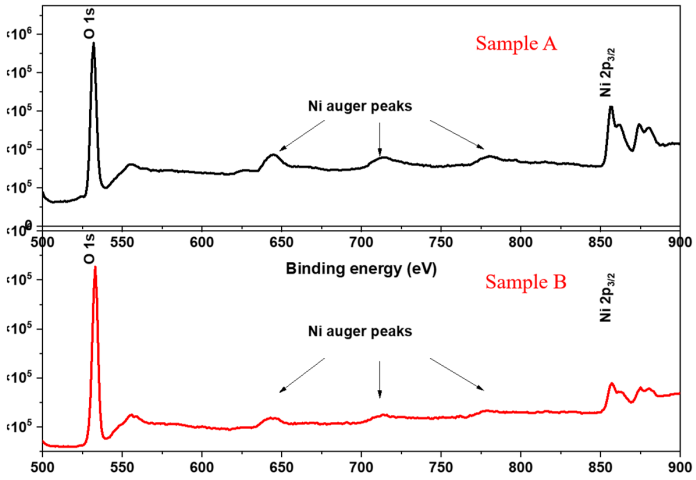

Figure S3: Corresponding XPS analyses of fs laser synthesis NiO nanoparticles Sample A and B, respectively.

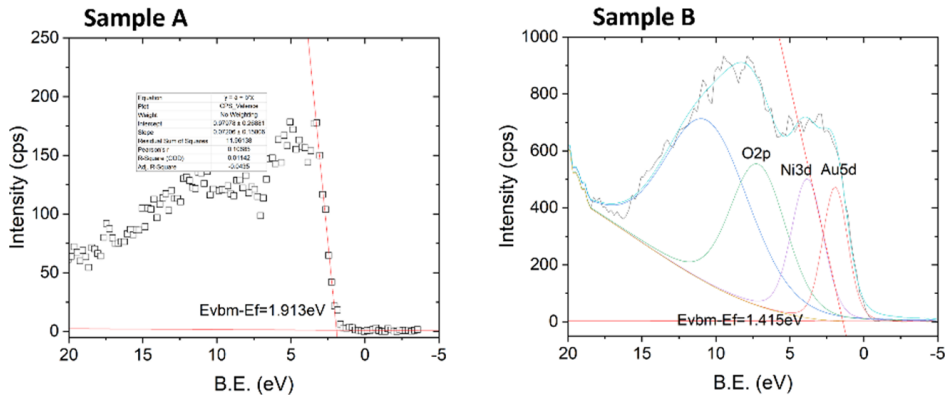

Figure S4: Valence band XPS evaluation data of NiO nanoparticles produced by fs laser when a Ni metallic target (Sample A) and when a NiO amorphous target (Sample B) was used.

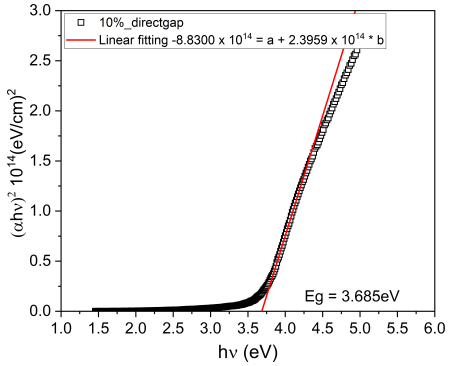

Figure S5: Optical band gap evaluation of NiO nanoparticles produced by microplasmas.

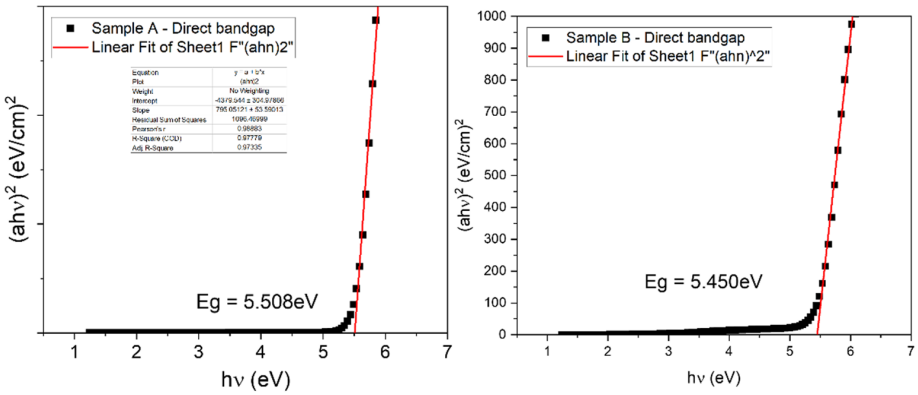

Figure S6: Optical band gap evaluation of NiO QDs produced by fs laser when a Ni metallic target (Sample A) and when a NiO amorphous target (Sample B) was used.

Band energy diagrams and Kelvin probe measurements.

The Kelvin probe (KP Technologies APS04) is operated in air with a 2 mm gold alloy tip, after calibrating the tip work function against a sputtered Au thin film[S1]. Additionally, the Kelvin probe (KP) setup is equipped with a surface photovoltage module which measures the surface contact potential difference (CPD) induced by a monochromated white light source and an air photoemission module, which uses a deuterium lamp source ($\Delta\lambda = 1$ nm) to induce photoemission of electrons from the samples.

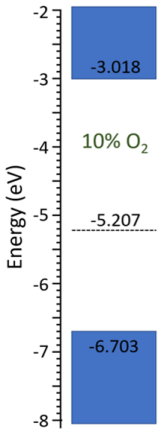

Figure S7: Energy band diagram of NiO nanoparticles with values of highest occupied molecular orbital (HOMO) and lowest unoccupied molecular orbital (LUMO). The Fermi Energy (dashed line) was determined by Kelvin probe measurements.

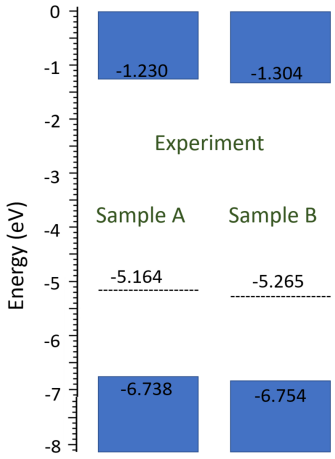

Figure S8: Energy band diagram of NiO nanoparticles with values of highest occupied molecular orbital (HOMO) and lowest unoccupied molecular orbital (LUMO). The Fermi Energy (dashed line) was determined by Kelvin probe measurements.

Details of first-principles calculations

All first-principles calculations are carried out with the quantum chemistry package Turbomole[S2] at the CAM-B3LYP level of theory[S3] employing a semi-numerical approximation for the exact-exchange contribution on the energy functional[S4]. We use the def2-TZVP basis set along with the corresponding density fitting basis[S5,S6]. All electronic structure calculations are converged with regard to the total energy change with a precision of 10^{-7} a.u.. All calculations are spin-unrestricted, where the initial guess for the wavefunction is prepared such that the magnetization is anti-ferromagnetic, with spin up on Ni atoms in sublattice A and spin down on sublattice B.

Wavefunctions of frontier orbitals

In figure S9 the wavefunctions of the 4 highest occupied and 4 lowest unoccupied frontier orbitals are summarized.

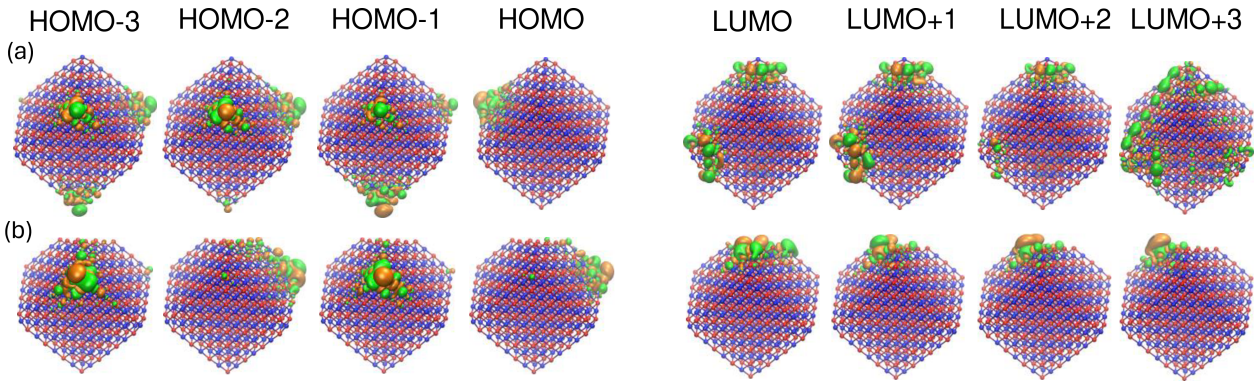

Figure S9: Wavefunctions of the occupied and unoccupied frontier orbitals for NiO nanocrystals ($d = 2.5\,\mathrm{nm}$) with (a) nonpolar and (b) polar surfaces. Here orange (green) indicates the isosurface of the wavefunction with positive (negative) sign.

Influence of the basis set on the orbital energies

In figure S10 we compare the dependence of the orbital energies on the size of the basis set, namely the small def2-SV(P) basis set and the fairly large def2-TZVP basis set. While the

orbital energies are overall shifted to lower energies the overall effect remains moderate and notably the HOMO-LUMO gap remains roughly unchanged.

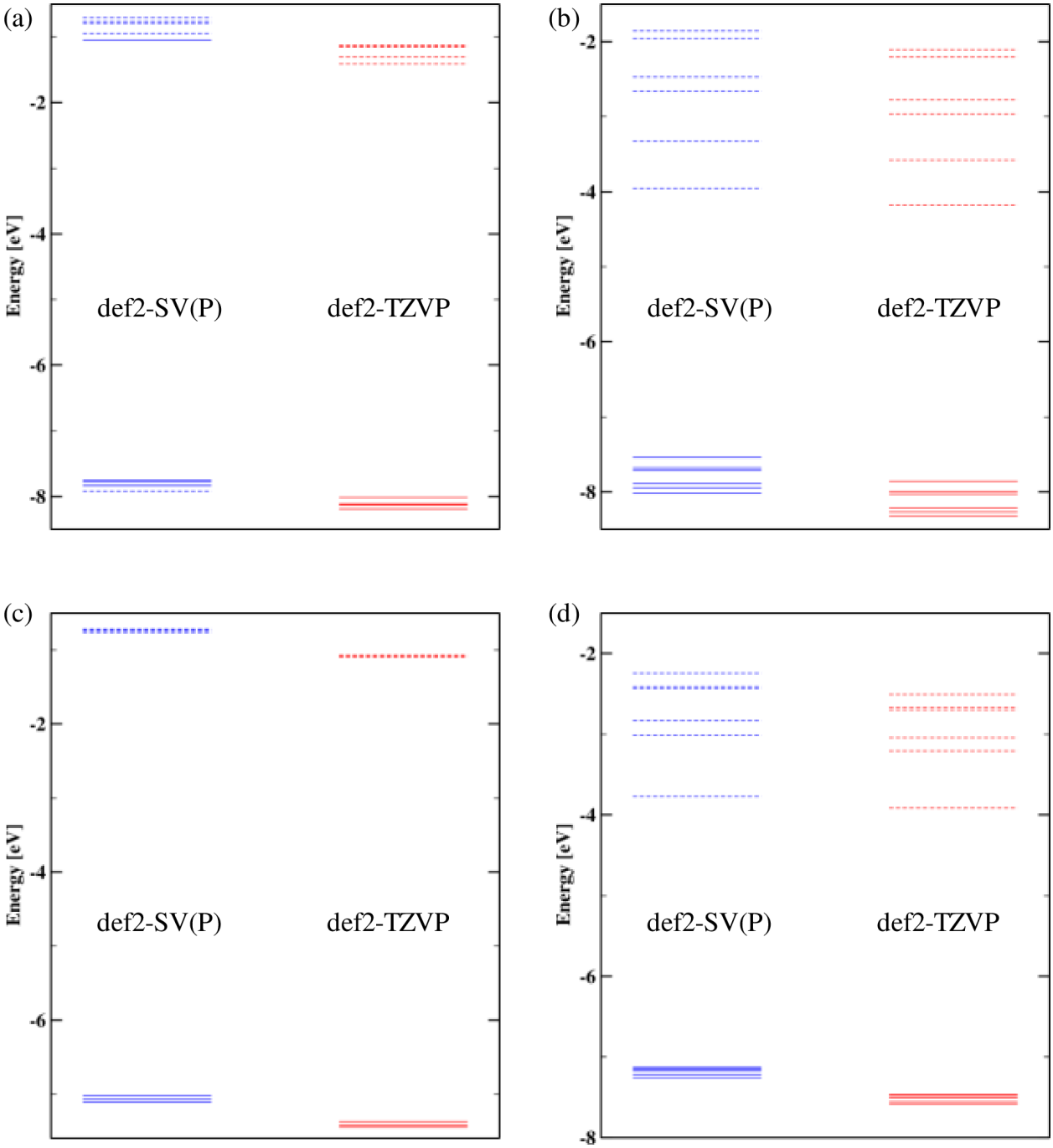

Figure S10: Comparison of the frontier orbital energies for the highest (lowest) occupied (unoccupied orbitals) for def2-SV(P) and def2-TZVP basis set for the NiO nanocrystals ($d = 1.1\,\mathrm{nm}$) with (a) nonpolar and (b) polar surfaces and for the NiO nanocrystals ($d = 2.5\,\mathrm{nm}$) with (c) nonpolar and (d) polar surfaces.

Table S1: Summary of the HOMO and LUMO energy as well as the HOMO-LUMO gap E_{gap} calculated using the def2-TZVP basis set of the small NiO nanocrystal ($d = 1.1\,nm$) with (a) nonpolar and (b) polar surfaces for different exchange-correlation functionals. In (b) the PBE calculation did produce a negative HOMO-LUMO gap and is not reported.

(a)	HOMO (eV)	LUMO (eV)	E_{gap}
PBE	-4.89	-4.70	0.19
HSE06	-6.22	-2.75	3.47
PBE0	-6.59	-2.31	4.28
CAM-B3LYP	-8.01	-1.41	6.60

(b)	HOMO (eV)	LUMO (eV)	E_{gap}
PBE	x	x	x
HSE06	-6.14	-5.32	0.82
PBE0	-6.50	-4.95	1.55
CAM-B3LYP	-7.86	-4.12	3.74

Exchange-correlation functional

In table S1 we compare the effect of different exchange correlation functionals, namely the semi-local PBE functional[S7,S8], the screened hybrid functional HSE06[S9–S11], the global hybrid PBE0 functional[S12,S13], and the long-range-corrected hybrid functional CAM-B3LYP[S3] for the small NiO nanocrystal ($d = 1.1\,nm$). While the absolute number differ between the hybrid functionals PBE0 and CAM-B3LYP, they produce the same overall trend when comparing nonpolar with polar nanocrystals and both predict the correct Mott insulating behavior of Nickel-Oxide. The pure functional PBE on the other hand fails to capture this and predicts a quasi-metallic behavior with a small HOMO-LUMO gap for the nonpolar nanocrystal and a negative HOMO-LUMO gap for the polar nanocrystal. The screened hybrid functional works HSE06 well for the nonpolar surface but performs rather poor for the polar surface which may be related to the difficulty to describe localized defect states[S14].

Cartesian coordinates of the structures

NiO ($d = 1.1$) nonpolar
Species x(Å) y(Å) z(Å)
Ni 2.81110 2.81110 2.81110
Ni -3.00951 -3.00951 -1.02887
Ni -1.01187 3.15184 -1.01187
Ni 1.02918 1.02918 -1.02918
Ni 1.02887 -3.00951 3.00952
Ni -2.81110 2.81110 -2.81110
Ni -1.01187 1.01187 -3.15184
Ni -3.15184 -1.01187 1.01187
Ni 1.01187 -1.01187 -3.15184
Ni -1.01187 -1.01187 3.15184
Ni -1.01187 -3.15184 1.01187
Ni 1.01187 3.15184 1.01187
Ni 3.15184 1.01187 1.01187
Ni 3.15184 -1.01187 -1.01187
Ni 2.81110 -2.81110 -2.81110
Ni -3.00952 1.02887 3.00951
O 0.99901 0.99901 -3.14865
O -1.05794 -1.05794 1.05794
O -1.05794 1.05794 -1.05794
O -0.99901 0.99901 3.14865
O -3.10121 0.99122 -3.10121
O -3.14865 0.99901 0.99901
O 3.10121 0.99122 3.10121
O -0.99901 -0.99901 -3.14865
O 1.05794 -1.05794 -1.05794
O 0.99901 -0.99901 3.14865
O 3.10121 -0.99122 -3.10121
O -3.10121 -0.99122 3.10121
O -3.14865 -0.99901 -0.99901
O 0.99122 -3.10121 -3.10121
O 3.14865 0.99901 -0.99901
O 3.14866 -0.99901 0.99901
O 0.99901 3.14865 -0.99901
O 3.00590 3.00590 -3.00590
O 3.10121 3.10121 0.99122
O 3.10121 -3.10121 -0.99122
O -0.99901 -3.14865 -0.99901
O -3.10121 -3.10121 0.99122
O -3.00590 -3.00590 -3.00590
O 1.05794 1.05794 1.05794
O -0.99122 -3.10121 3.10121
O 0.99122 3.10121 3.10121
O 0.99901 -3.14865 0.99901
O -0.99901 3.14865 0.99901
O -0.99122 3.10121 -3.10121
O -3.10121 3.10121 -0.99122
O -3.00590 3.00590 3.00590
O 3.00590 -3.00591 3.00590
Ni 3.00951 1.02887 -3.00951
Ni -1.02887 -3.00951 -3.00951
Ni 3.00951 -3.00951 1.02887
Ni 1.02918 -1.02918 1.02918
Ni -2.81110 -2.81110 2.81110
Ni 1.02887 3.00951 -3.00951
Ni -3.00951 -1.02887 -3.00951
Ni 1.01187 1.01187 3.15184
Ni -3.15184 1.01187 -1.01187
Ni -3.00952 3.00951 1.02887
Ni -1.02917 1.02918 1.02917
Ni 3.00951 -1.02887 3.00951
Ni 3.00951 3.00951 -1.02887
Ni -1.02918 -1.02918 -1.02918
Ni -1.02887 3.00952 3.00951
Ni 1.01187 -3.15184 -1.01187

NiO ($d = 2.5$) nonpolar
Species x(Å) y(Å) z(Å)
Ni -1.04658 -1.04658 -1.04658
Ni -7.33689 1.03450 3.10062
Ni 1.03913 3.12426 5.24191
Ni -1.03554 -1.03554 7.34932
Ni 7.34931 -1.03554 -1.03554
Ni 7.16849 -1.02902 7.16849
Ni -1.03554 7.34931 -1.03554
Ni -1.02902 7.16849 7.16849
Ni 7.16849 7.16849 -1.02901
Ni 6.91007 6.91007 6.91007
Ni -7.11728 -7.11727 -5.09392
Ni -7.15082 -7.15082 3.04171
Ni 1.02736 -7.31741 -5.17129
Ni 1.03450 -7.33689 3.10062
Ni 5.16764 5.16764 -5.16764
Ni -7.31741 1.02736 -5.17129
Ni -3.11472 5.23132 3.11473
Ni 1.04476 1.04476 3.14507
Ni -5.24190 -1.03913 3.12426
Ni 3.12426 -1.03913 -5.24190
Ni 3.13734 -1.04210 3.13734
Ni -5.12430 7.29928 -5.12430
Ni -5.16225 7.30245 3.08275
Ni 3.08275 7.30246 -5.16225

Ni 3.09222 7.32571 3.09222
Ni -3.11472 -3.11472 -5.23132
Ni -3.13130 -3.13130 3.13130
Ni 5.20523 -3.10837 -5.20523
Ni 5.23132 -3.11473 3.11473
Ni 1.03883 1.03883 -5.25198
Ni -5.21017 -1.03033 -5.21018
Ni -3.10062 -7.33689 -1.03450
Ni 5.20523 5.20523 3.10837
Ni -7.16849 -1.02901 -7.16849
Ni -7.16849 7.16849 1.02902
Ni -6.91007 6.91007 -6.91007
Ni 1.04658 -1.04658 1.04658
Ni 1.03554 -1.03554 -7.34932
Ni -7.34931 -1.03554 1.03554
Ni 5.17129 -7.31741 -1.02736
Ni 5.17129 1.02736 7.31741
Ni 5.25198 1.03883 -1.03883
Ni -3.10063 1.03449 7.33688
Ni -3.14507 1.04476 -1.04476
Ni 5.09391 -7.11728 7.11728
Ni 1.02902 7.16849 -7.16849
Ni -3.04171 -7.15082 7.15082
Ni -7.30246 3.08275 5.16225
Ni -5.12430 5.12430 -7.29928
Ni 1.03554 7.34931 1.03553

Ni -5.16225 -3.08274 -7.30246
Ni -5.24190 -3.12426 1.03913
Ni 3.09222 -3.09221 -7.32571
Ni 3.13734 -3.13734 1.04210
Ni -5.21017 5.21017 1.03033
Ni 3.08275 5.16226 -7.30245
Ni 3.12426 5.24190 1.03913
Ni -7.30245 -5.16225 -3.08275
Ni -7.29928 -5.12430 5.12430
Ni 1.03913 -5.24190 -3.12426
Ni 1.03032 -5.21017 5.21017
Ni -7.32571 3.09222 -3.09222
Ni -3.10837 5.20523 -5.20523
Ni 1.04211 3.13734 -3.13734
Ni -3.08275 7.30245 5.16226
Ni -3.08275 -5.16225 -7.30246
Ni 3.09222 3.09222 7.32571
Ni 5.12430 -5.12430 -7.29928
Ni 5.21018 -5.21018 1.03033
Ni -3.09222 3.09222 -7.32571
Ni -3.13734 3.13734 1.04210
Ni 5.16226 3.08275 -7.30245
Ni 5.24190 3.12426 1.03913
Ni -5.21017 -5.21017 -1.03033
Ni -5.12430 -5.12430 7.29928
Ni 3.12426 -5.24190 -1.03913

Ni 3.08274 -5.16225 7.30245
Ni -5.24190 3.12426 -1.03913
Ni 3.13734 3.13734 -1.04210
Ni 5.12430 7.29928 5.12430
Ni -5.16225 -7.30246 -3.08275
Ni -5.12430 -7.29928 5.12430
Ni 3.09222 -7.32571 -3.09222
Ni 3.08274 -7.30245 5.16225
Ni -5.24190 1.03913 -3.12426
Ni -5.21018 1.03033 5.21017
Ni 3.13734 1.04210 -3.13734
Ni 3.12426 1.03913 5.24190
Ni -3.13734 -1.04211 -3.13734
Ni -3.12426 -1.03913 5.24190
Ni 5.24190 -1.03913 -3.12426
Ni 5.21017 -1.03033 5.21017
Ni -3.09221 7.32571 -3.09222
Ni 1.02736 5.17129 7.31741
Ni 5.16225 7.30246 -3.08275
Ni -1.04210 -3.13734 -3.13734
Ni -5.16225 3.08275 7.30246
Ni 1.03883 5.25198 -1.03883
Ni -1.03913 -3.12426 5.24190
Ni 7.32571 -3.09221 -3.09222
Ni 7.30245 -3.08275 5.16225
Ni -1.03913 5.24190 -3.12426

Ni -1.03033 5.21017 5.21017
Ni 7.30246 5.16225 -3.08274
Ni 7.29928 5.12430 5.12430
Ni -1.03033 -5.21018 -5.21018
Ni -1.03913 -5.24190 3.12426
Ni 7.30245 -5.16225 3.08275
Ni -1.03912 3.12426 -5.24190
Ni -1.04211 3.13734 3.13734
Ni 7.30246 3.08275 -5.16225
Ni 7.32571 3.09222 3.09222
Ni 7.29928 -5.12430 -5.12430
Ni -3.12427 -5.24190 1.03913
Ni -7.11728 5.09391 7.11728
Ni -1.02901 -7.16849 -7.16849
Ni 1.03450 -3.10062 7.33688
Ni 1.04476 -3.14507 -1.04476
Ni -7.15082 -3.04171 7.15082
Ni -7.33689 -3.10062 -1.03450
Ni 7.34932 1.03554 1.03554
Ni -7.31741 5.17129 -1.02737
Ni -1.04658 1.04658 1.04658
Ni -1.03554 1.03554 -7.34931
Ni 7.16849 -7.16849 1.02902
Ni 6.91007 -6.91007 -6.91007
Ni -1.03554 -7.34931 1.03554
Ni 7.16849 1.02902 -7.16849

O 1.02418 7.21321 7.21321
O -1.03270 -7.35165 -1.03270
O -1.02419 -7.21321 7.21321
O 7.21321 -7.21321 -1.02419
O 7.06976 -7.06976 7.06976
O 7.35165 1.03270 -1.03270
O -1.03271 1.03270 7.35165
O 7.21321 1.02418 7.21322
O -3.13747 -1.04593 3.13748
O 1.03270 -1.03270 7.35166
O 1.03270 7.35165 -1.03270
O -1.04841 1.04841 -1.04841
O -7.06976 7.06976 7.06976
O 3.07435 7.20582 -7.20581
O 1.04841 -1.04841 -1.04841
O -5.09115 7.21102 -7.21101
O -7.21321 -1.02419 7.21321
O -7.35166 -1.03270 -1.03270
O 1.03090 7.34216 3.10393
O 1.02768 7.32643 -5.14557
O -7.20582 7.20581 3.07435
O -7.21101 7.21101 -5.09116
O 1.04585 -1.04585 3.14226
O 1.04268 -1.04267 -5.25450
O -7.34216 -1.03090 3.10392
O -7.32643 -1.02768 -5.14557

O 3.10392 7.34216 1.03090
O 3.14226 -1.04585 1.04585
O -7.21321 7.21321 -1.02419
O 3.10392 -1.03089 -7.34216
O -5.09116 -7.21102 7.21101
O 3.07435 -7.20582 7.20582
O -5.14557 7.32644 1.02769
O -5.14557 -1.02768 -7.32644
O 3.09674 7.33213 -3.09674
O -5.10613 7.28724 5.10613
O -5.13709 7.32037 -3.08435
O 3.12015 -1.03608 5.24328
O 3.13748 -1.04593 -3.13748
O -5.21823 -1.03956 5.21822
O -5.24328 -1.03607 -3.12016
O 5.21823 1.03955 5.21823
O 5.24328 1.03608 -3.12015
O -3.12015 1.03608 5.24328
O -3.13748 1.04593 -3.13748
O 5.10613 -7.28724 5.10613
O 5.13709 -7.32037 -3.08435
O -3.08435 -7.32037 5.13709
O -3.09674 -7.33213 -3.09674
O 5.09116 7.21101 7.21102
O 5.14557 7.32643 -1.02768
O -3.07435 7.20582 7.20582

O -3.10392 7.34216 -1.03090
O 5.14557 -1.02769 7.32643
O 5.25450 -1.04267 -1.04267
O -3.10392 -1.03090 7.34216
O -3.14226 -1.04585 -1.04585
O 3.10392 1.03089 7.34216
O 3.14226 1.04585 -1.04585
O -5.14557 1.02768 7.32643
O -5.25450 1.04267 -1.04268
O -5.25450 -1.04268 1.04267
O 3.10392 -7.34216 -1.03090
O 5.24328 -1.03608 3.12015
O -5.14557 -7.32644 -1.02768
O 3.08435 -7.32037 -5.13710
O -3.09575 5.20414 5.20414
O -3.12164 5.23477 -3.12165
O 5.20414 -3.09575 5.20415
O 5.23478 -3.12164 -3.12164
O -3.12165 -3.12164 5.23478
O -3.12982 -3.12982 -3.12981
O 1.04840 1.04841 1.04840
O 1.03270 1.03271 -7.35165
O -7.35165 1.03270 1.03271
O -7.21321 1.02419 -7.21322
O 1.03270 -7.35165 1.03270
O 1.02419 -7.21321 -7.21321

O -7.06976 -7.06976 -7.06976
O -7.21321 -7.21321 1.02419
O 1.04267 1.04267 5.25450
O -7.20582 -7.20582 -3.07435
O 1.04585 1.04585 -3.14225
O 3.09673 -7.33213 3.09674
O -5.21822 1.03956 -5.21823
O -5.24328 1.03608 3.12015
O 3.13747 1.04593 3.13748
O 3.12015 1.03608 -5.24328
O -7.21102 -7.21102 5.09115
O 1.03090 -7.34216 -3.10392
O 1.02768 -7.32643 5.14557
O -7.34216 1.03090 -3.10392
O -3.12015 -1.03607 -5.24328
O 5.20414 5.20414 -3.09575
O -5.13710 -7.32037 3.08435
O 5.21822 -1.03955 -5.21822
O 7.34216 1.03090 3.10392
O -5.10613 -7.28724 -5.10613
O 7.32643 1.02769 -5.14557
O -1.04585 1.04585 3.14226
O -1.04267 1.04268 -5.25450
O 7.20582 -7.20582 3.07435
O 7.21102 -7.21101 -5.09116
O -1.03090 -7.34216 3.10392

O -1.02769 -7.32644 -5.14557
O 7.21101 7.21101 5.09116
O 7.20582 7.20582 -3.07435
O -1.02769 7.32643 5.14557
O -1.03089 7.34216 -3.10392
O 7.32643 -1.02769 5.14557
O 7.34216 -1.03090 -3.10392
O -1.04268 -1.04267 5.25450
O -1.04585 -1.04585 -3.14225
O 7.21321 7.21321 1.02419
O 7.06976 7.06976 -7.06976
O -1.03270 7.35165 1.03270
O -1.02418 7.21321 -7.21321
O 7.35165 -1.03271 1.03271
O 7.21321 -1.02419 -7.21321
O -1.04841 -1.04841 1.04841
O -1.03270 -1.03270 -7.35165
O 5.13710 7.32037 3.08435
O 5.10613 7.28724 -5.10613
O -3.09674 7.33213 3.09674
O -3.08435 7.32037 -5.13710
O 5.20176 5.20176 5.20176
O 3.08435 7.32037 5.13710
O -7.32644 1.02768 5.14557
O 7.32037 3.08435 5.13710
O -7.34216 -3.10392 1.03090

O -7.28724 -5.10613 -5.10613
O 3.13748 3.13747 1.04594
O -1.04593 3.13747 -3.13748
O 7.28724 -5.10613 5.10613
O 7.32037 -5.13709 -3.08435
O -1.03956 -5.21823 5.21823
O -1.03608 -5.24328 -3.12015
O 7.32037 5.13710 3.08435
O 7.28724 5.10613 -5.10613
O -1.03607 5.24328 3.12015
O -1.03955 5.21823 -5.21822
O 7.33213 -3.09674 3.09674
O 7.32037 -3.08434 -5.13710
O -1.03607 3.12015 5.24328
O -1.04593 -3.13748 3.13748
O 5.25450 1.04268 1.04267
O 5.14557 1.02769 -7.32643
O -3.14226 1.04585 1.04585
O -3.10392 1.03090 -7.34216
O 5.14557 -7.32643 1.02768
O 5.09116 -7.21101 -7.21101
O -3.10392 -7.34216 1.03089
O -3.07435 -7.20582 -7.20582
O 1.04593 3.13748 3.13747
O 1.03608 3.12015 -5.24328
O -7.33213 3.09674 3.09674

O -7.32037 3.08435 -5.13710
O 1.03607 -5.24328 3.12015
O -1.03608 -3.12015 -5.24328
O 1.03956 -5.21822 -5.21823
O -3.08435 -5.13710 7.32037
O 5.20176 -5.20175 -5.20176
O 7.33213 3.09674 -3.09674
O 7.34215 3.10392 1.03090
O 7.21102 -5.09115 -7.21101
O 7.32643 -5.14557 1.02769
O -1.03089 3.10392 -7.34216
O -1.04585 3.14226 1.04585
O 7.20582 3.07435 -7.20582
O -7.21102 -5.09116 7.21101
O -7.32644 -5.14557 -1.02769
O -1.02768 -5.14557 -7.32644
O 1.04267 -5.25451 -1.04268
O 1.02768 -5.14557 7.32643
O -7.34216 3.10392 -1.03090
O -3.12164 -5.23478 3.12164
O -7.20582 3.07435 7.20582
O -3.09674 3.09673 7.33213
O 5.13709 3.08435 7.32037
O 5.24328 3.12015 -1.03608
O -3.13748 3.13747 -1.04593
O 5.10613 -5.10613 7.28724

O 5.21822 -5.21822 -1.03956
O 1.04585 3.14225 -1.04584
O -3.12016 -5.24328 -1.03608
O 5.23478 3.12165 3.12165
O 5.20414 3.09575 -5.20414
O -3.12982 3.12981 3.12982
O -3.12164 3.12164 -5.23478
O 5.20414 -5.20414 3.09575
O -1.04267 -5.25450 1.04267
O -7.32037 -5.13710 3.08435
O 1.03090 3.10392 7.34216
O -7.20582 -3.07435 -7.20582
O -5.24328 3.12015 1.03608
O 1.03955 5.21822 5.21823
O -5.13710 3.08435 -7.32037
O 3.12015 -5.24328 1.03608
O 3.08435 -5.13709 -7.32037
O -5.21823 -5.21823 1.03955
O -5.10613 -5.10613 -7.28724
O 7.21101 5.09115 7.21101
O 7.32643 5.14557 -1.02768
O -1.02769 5.14557 7.32643
O -1.04267 5.25450 -1.04267
O 7.20582 -3.07435 7.20582
O -1.03090 -3.10392 7.34216
O -1.04585 -3.14225 -1.04585

O 1.03608 5.24329 -3.12015
O 3.08435 5.13709 7.32037
O -7.28724 5.10613 5.10613
O -7.32037 5.13710 -3.08435
O 1.03607 -3.12016 5.24328
O 1.04594 -3.13747 -3.13747
O -7.32037 -3.08435 5.13709
O -7.33213 -3.09674 -3.09674
O 1.04267 5.25450 1.04267
O 1.02769 5.14557 -7.32643
O -7.32643 5.14556 1.02769
O -7.21101 5.09116 -7.21101
O 1.04585 -3.14225 1.04585
O -3.09575 -5.20414 -5.20414
O 1.03090 -3.10392 -7.34216
O 3.12015 5.24328 -1.03608
O -5.21822 5.21823 -1.03956
O 7.34216 -3.10392 -1.03090
O 3.12983 3.12982 -3.12982
O 3.09674 3.09674 -7.33213
O -3.09674 -3.09674 -7.33213
O 3.09674 -3.09674 7.33213
O 3.13747 -3.13748 -1.04593
O -5.13710 -3.08435 7.32037
O -5.24328 -3.12016 -1.03608
O 3.12165 5.23478 3.12165

O 3.09575 5.20414 -5.20414
O -5.20414 5.20414 3.09575
O 3.12981 -3.12982 3.12982
O 3.12164 -3.12164 -5.23478
O -5.23478 -3.12164 3.12164
O -5.20414 -3.09575 -5.20414
O 3.12164 3.12164 5.23478
O -5.20176 5.20176 -5.20176
O -5.10613 5.10613 7.28724
O -3.13747 -3.13747 1.04593
O -5.20414 3.09574 5.20414
O 5.24328 -3.12015 1.03608
O -3.08434 5.13710 -7.32037
O -3.12015 5.24328 1.03608
O 5.10613 5.10613 -7.28724
O 5.21822 5.21822 1.03955
O 5.13710 -3.08434 -7.32037
O -5.20176 -5.20176 5.20176
O 3.12164 -5.23478 -3.12164
O 3.09575 -5.20414 5.20414
O -5.23478 3.12164 -3.12164
O -5.20414 -5.20415 -3.09575
Ni 3.04171 -7.15081 -7.15082
Ni -5.17129 -7.31741 1.02736
Ni -5.09391 -7.11728 -7.11728
Ni 7.31741 5.17129 1.02737

Ni 7.11728 5.09392 -7.11728
Ni -1.03883 5.25197 1.03884
Ni 7.33688 -3.10062 1.03450
Ni 7.15082 -3.04170 -7.15082
Ni -1.04476 -3.14507 1.04476
Ni 5.21018 1.03033 -5.21018
Ni -5.25198 1.03883 1.03883
Ni 3.10062 -7.33688 1.03450
Ni -1.02736 5.17129 -7.31741
Ni -5.17129 1.02736 -7.31741
Ni 5.20523 -5.20523 -3.10837
Ni -3.13129 3.13129 -3.13129
Ni 3.14507 1.04475 1.04476
Ni -1.03450 -7.33689 -3.10062
Ni -1.02737 -7.31741 5.17129
Ni 7.15082 -7.15082 -3.04171
Ni 7.11727 -7.11728 5.09392
Ni -1.04475 1.04476 -3.14507
Ni -1.03883 1.03883 5.25197
Ni 7.33689 1.03450 -3.10062
Ni 7.31741 1.02736 5.17129
Ni -3.11472 -5.23132 -3.11473
Ni -3.10838 -5.20523 5.20523
Ni -3.11473 3.11472 5.23132
Ni 3.10062 1.03450 -7.33688
Ni 5.23132 3.11473 -3.11473

Ni 5.21018 5.21018 -1.03033
Ni -3.12426 5.24190 -1.03913
Ni 5.16764 -5.16764 5.16764
Ni -7.16849 -7.16849 -1.02902
Ni -6.91008 -6.91008 6.91007
Ni 1.03554 -7.34931 -1.03554
Ni 1.02901 -7.16849 7.16849
Ni -7.34931 1.03554 -1.03554
Ni -7.16849 1.02901 7.16849
Ni 1.04658 1.04658 -1.04658
Ni 1.03554 1.03553 7.34931
Ni -3.10062 -1.03450 -7.33689
Ni -3.14507 -1.04476 1.04475
Ni 5.17129 -1.02736 -7.31741
Ni 5.25198 -1.03883 1.03883
Ni -3.04170 7.15082 -7.15082
Ni -3.10062 7.33688 1.03450
Ni 5.09392 7.11728 -7.11728
Ni 5.17129 7.31741 1.02737
Ni -7.11728 -5.09391 -7.11728
Ni -7.31741 -5.17129 1.02736
Ni 1.02736 -5.17129 -7.31741
Ni 1.03883 -5.25198 1.03883
Ni -7.15081 3.04171 -7.15082
Ni -7.33689 3.10062 1.03450
Ni 1.03450 3.10062 -7.33688

Ni 1.04476 3.14507 1.04476
Ni -3.13734 -3.13734 -1.04211
Ni -3.09222 -3.09222 7.32571
Ni 5.24190 -3.12425 -1.03913
Ni 5.16225 -3.08275 7.30246
Ni 5.20523 3.10837 5.20523
Ni -3.08275 5.16225 7.30246
Ni -5.20523 -3.10838 5.20523
Ni 5.12430 5.12430 7.29928
Ni -1.03450 3.10062 7.33689
Ni 1.03913 -3.12425 -5.24190
Ni 1.04210 -3.13734 3.13734
Ni -7.29928 5.12430 -5.12430
Ni -7.30246 5.16225 3.08274
Ni 1.03033 5.21017 -5.21017
Ni 1.03913 5.24190 3.12426
Ni -7.33689 -1.03450 -3.10062
Ni -7.31741 -1.02736 5.17129
Ni 1.04476 -1.04476 -3.14507
Ni 1.03883 -1.03883 5.25198
Ni -7.15082 7.15082 -3.04171
Ni -7.11728 7.11727 5.09392
Ni 1.02736 7.31741 5.17129
Ni 1.03450 7.33689 -3.10062
Ni -5.23132 -3.11473 -3.11473
Ni 3.10838 5.20523 5.20523

Ni -1.04476 3.14507 -1.04476
Ni 7.11727 -5.09392 7.11727
Ni 7.31741 -5.17129 -1.02736
Ni -1.02737 -5.17129 7.31741
Ni -1.03883 -5.25197 -1.03883
Ni -7.30245 -3.08274 -5.16225
Ni 3.11472 5.23133 -3.11472
Ni -5.20523 5.20523 -3.10837
Ni 3.11473 -3.11473 5.23132
Ni 3.13129 -3.13129 -3.13130
Ni -5.16764 5.16764 5.16764
Ni -7.32571 -3.09222 3.09221
Ni 7.33689 3.10062 -1.03450
Ni -5.23132 3.11473 3.11473
Ni -1.03883 -1.03883 -5.25198
Ni 3.13129 3.13130 3.13130

Ni -1.04476 -1.04476 3.14507
Ni 7.31741 -1.02736 -5.17129
Ni 7.33688 -1.03450 3.10062
Ni -1.02736 7.31741 -5.17129
Ni -1.03450 7.33689 3.10062
Ni 7.11728 7.11728 -5.09391
Ni 7.15082 7.15082 3.04171
Ni -5.16764 -5.16764 -5.16764
Ni -5.20523 -5.20523 3.10837
Ni 3.10837 -5.20523 -5.20523
Ni 3.11473 -5.23133 3.11473
Ni -5.20523 3.10837 -5.20523
Ni 3.11473 3.11473 -5.23132
Ni -5.25198 -1.03884 -1.03883
Ni 7.15082 3.04171 7.15082
Ni -5.17129 -1.02737 7.31741

Ni 3.14507 -1.04476 -1.04476
Ni 3.10062 -1.03450 7.33689
Ni -5.17129 7.31741 -1.02736
Ni -5.09392 7.11727 7.11728
Ni 3.10063 7.33689 -1.03449
Ni 3.04170 7.15082 7.15082
Ni -3.08275 -7.30245 -5.16225
Ni -3.09222 -7.32571 3.09222
Ni 5.12430 -7.29928 -5.12430
Ni 5.16225 -7.30245 3.08274
Ni -3.12426 1.03913 -5.24190
Ni -3.13734 1.04210 3.13734
Ni -1.03450 -3.10062 -7.33689
Ni 5.24190 1.03913 3.12426

NiO ($d = 2.5$) polar
Species x(Å) y(Å) z(Å)
Ni -0.90478 -1.19023 -1.20456
Ni -7.17658 0.88111 2.94479
Ni 1.18315 2.96977 5.10733
Ni -0.89431 -1.17401 7.15149
Ni 7.50168 -1.18700 -1.18247
Ni 7.37798 -1.18894 6.99396
Ni -0.88171 7.18969 -1.19325
Ni -0.87851 7.07313 7.02593
Ni 7.36074 7.02355 -1.18344
Ni 7.11808 6.78765 6.72824
Ni -6.92560 -7.24871 -5.26688
Ni -7.06684 -7.22614 2.90178
Ni 1.17751 -7.45807 -5.34508
Ni 1.17761 -7.45580 2.95613
Ni 5.35373 5.06028 -5.27830
Ni -7.19357 0.87495 -5.29033
Ni -2.94167 5.13357 2.94255
Ni 1.19303 0.89073 2.98247
Ni -5.11867 -1.17878 3.00043
Ni 3.25384 -1.17873 -5.41215
Ni 3.30554 -1.18104 2.99370
Ni -4.99838 7.14494 -5.30609
Ni -5.06327 7.17475 2.93273
Ni 3.24143 7.10887 -5.30213

Ni 3.24615 7.23138 2.93391
Ni -2.95876 -3.25984 -5.43078
Ni -2.99214 -3.28822 2.99763
Ni 5.31516 -3.25767 -5.37110
Ni 5.41448 -3.24042 2.93731
Ni 1.19713 0.89398 -5.40815
Ni -5.01373 -1.16676 -5.34830
Ni -2.95706 -7.50281 -1.19417
Ni 5.37452 5.05379 2.98499
Ni -7.06094 -1.18826 -7.35262
Ni -6.97639 6.96178 0.87850
Ni -6.77098 6.76413 -7.04049
Ni 1.18738 -1.19354 0.90626
Ni 1.18323 -1.19447 -7.45968
Ni -7.15984 -1.18330 0.88426
Ni 5.36209 -7.42868 -1.17549
Ni 5.32214 0.87477 7.18011
Ni 5.42734 0.89330 -1.19385
Ni -2.95256 0.88598 7.25067
Ni -2.99277 0.89020 -1.18325
Ni 5.25890 -7.33024 6.93928
Ni 1.18063 6.98189 -7.33751
Ni -2.87932 -7.28503 7.00640
Ni -7.20416 2.92638 4.97565
Ni -4.98575 5.00060 -7.50019
Ni 1.19462 7.22492 0.88829

Ni -4.97619 -3.22245 -7.50728
Ni -5.05853 -3.26808 0.89319
Ni 3.26000 -3.20869 -7.51351
Ni 3.29138 -3.30111 0.88754
Ni -5.10665 5.05171 0.87897
Ni 3.23330 5.00543 -7.47697
Ni 3.30259 5.04837 0.88855
Ni -7.14244 -5.28570 -3.23892
Ni -7.10398 -5.28417 4.98455
Ni 1.18877 -5.36147 -3.24087
Ni 1.17235 -5.37025 5.03672
Ni -7.13346 2.95793 -3.25787
Ni -2.98736 5.00674 -5.38907
Ni 1.19155 2.98908 -3.31604
Ni -2.93753 7.21781 5.01831
Ni -2.95782 -5.36085 -7.39166
Ni 3.25093 2.96125 7.22414
Ni 5.39850 -5.38130 0.88648
Ni -2.94878 2.93435 -7.41132
Ni -3.01075 3.01705 0.89196
Ni 5.28613 2.96087 -7.41521
Ni 5.35257 2.94943 0.89121
Ni -5.09133 -5.38188 -1.17632
Ni -4.93212 -5.28921 7.10364
Ni 3.27258 -5.36274 -1.19134
Ni 3.26007 -5.31512 7.20804

Ni -5.13074 2.97928 -1.17593
Ni 3.29338 2.99528 -1.18200
Ni 5.24431 7.11568 4.98331
Ni -5.01723 -7.42992 -3.24707
Ni -5.01157 -7.49549 4.93034
Ni 3.25810 -7.45949 -3.22515
Ni 3.20936 -7.40509 5.02809
Ni -5.05975 0.88853 -3.25031
Ni -5.06260 0.88773 5.08470
Ni 3.30208 0.89832 -3.28120
Ni 3.29701 0.88760 5.04336
Ni -2.96543 -1.17853 -3.31693
Ni -2.96740 -1.19107 5.13875
Ni 5.39588 -1.19520 -3.29695
Ni 5.40006 -1.17951 5.01391
Ni -2.95786 7.15598 -3.26741
Ni 1.17156 5.02343 7.10432
Ni 5.31666 7.12868 -3.20891
Ni -0.89809 -3.28212 -3.29278
Ni -5.02857 2.91904 7.09087
Ni 1.17599 5.14924 -1.19267
Ni -0.89813 -3.25589 5.13027
Ni 7.53585 -3.23505 -3.26118
Ni 7.49572 -3.26097 4.98495
Ni -0.89175 5.12690 -3.28563
Ni -0.87477 5.10750 5.07676

Ni 7.48956 4.96625 -3.20740
Ni 7.37782 4.94921 4.93516
Ni -0.87753 -5.32625 -5.39649
Ni -0.89687 -5.42404 2.96820
Ni 7.45369 -5.35197 2.91623
Ni -0.89737 2.95542 -5.37972
Ni -0.89641 3.01772 2.97152
Ni 7.41157 2.94924 -5.32300
Ni 7.40646 2.93140 2.94442
Ni -2.99695 -5.41658 0.89827
Ni -7.02846 4.98372 6.93241
Ni -0.88286 -7.28178 -7.36876
Ni 1.18475 -3.25938 7.15912
Ni 1.18763 -3.27912 -1.18636
Ni -6.97459 -3.16901 6.96621
Ni -7.24759 -3.24499 -1.17965
Ni 7.56756 0.88517 0.88720
Ni -7.16003 4.98481 -1.17846
Ni -0.89295 0.89660 0.89815
Ni -0.89480 0.88677 -7.54989
Ni 7.38434 -7.32164 0.88456
Ni -0.88204 -7.55959 0.88991
Ni 7.31060 0.88251 -7.32290
O 1.18207 7.03689 7.08859
O -0.88252 -7.52271 -1.19136
O -0.87151 -7.30019 7.09740

O 7.29842 -7.39823 -1.17724
O 7.28535 -7.22967 6.90310
O 7.51504 0.88669 -1.17338
O -0.88433 0.87916 7.22337
O 7.39213 0.88157 6.99614
O -2.96433 -1.18970 3.01531
O 1.17581 -1.18960 7.16471
O 1.17160 7.16618 -1.19091
O -0.90441 0.89382 -1.19568
O -6.93476 6.92014 6.88046
O 3.21042 7.00285 -7.29979
O 1.19190 -1.20198 -1.18622
O -4.91520 7.09885 -7.37973
O -7.02995 -1.16144 6.99734
O -7.17031 -1.17949 -1.19268
O 1.16830 7.25711 2.96670
O 1.18657 7.13204 -5.33368
O -7.12487 7.03652 2.94856
O -7.09617 7.02232 -5.21363
O 1.20255 -1.20211 3.00203
O 1.19889 -1.19788 -5.37192
O -7.17988 -1.17640 2.96665
O -7.19266 -1.17995 -5.24389
O 3.27197 7.16120 0.87488
O 3.28214 -1.18689 0.89157
O -7.03283 7.08675 -1.18083

O 3.24551 -1.17740 -7.50378
O -4.89717 -7.40668 7.02095
O 3.23508 -7.40802 7.02200
O -4.98877 7.15881 0.87817
O -4.96266 -1.17825 -7.54514
O 3.23848 7.16596 -3.26311
O -4.96442 7.08595 4.94177
O -5.01524 7.14959 -3.25933
O 3.27385 -1.18083 5.14391
O 3.26030 -1.18754 -3.28493
O -5.06999 -1.19184 5.03377
O -5.08098 -1.18569 -3.26345
O 5.38002 0.89319 5.02566
O 5.41748 0.89443 -3.28133
O -2.98791 0.88808 5.12109
O -2.96680 0.89039 -3.30928
O 5.22987 -7.48710 4.94524
O 5.30829 -7.46011 -3.22650
O -2.94994 -7.39596 4.98196
O -2.95142 -7.50737 -3.24658
O 5.26373 7.04654 7.04561
O 5.33304 7.21143 -1.17184
O -2.94541 7.08331 6.99515
O -2.92645 7.19502 -1.17914
O 5.34340 -1.18521 7.11821
O 5.36772 -1.19030 -1.19185

O -2.96580 -1.18762 7.17092
O -2.97653 -1.20076 -1.20530
O 3.28081 0.87926 7.23463
O 3.32095 0.89227 -1.20478
O -5.04152 0.87936 7.20393
O -5.06900 0.88574 -1.18993
O -5.06724 -1.19377 0.89925
O 3.28423 -7.49941 -1.17788
O 5.36594 -1.19458 2.96479
O -5.01397 -7.51365 -1.18565
O 3.20103 -7.48137 -5.27748
O -2.92696 5.08704 5.03061
O -2.97932 5.13015 -3.24446
O 5.36725 -3.24142 5.08082
O 5.34855 -3.28415 -3.24274
O -2.98373 -3.25731 5.08999
O -2.96832 -3.26641 -3.30990
O 1.20571 0.90083 0.90091
O 1.17015 0.88848 -7.55848
O -7.18174 0.88832 0.87620
O -7.10164 0.87471 -7.37256
O 1.17464 -7.56117 0.88392
O 1.18165 -7.32080 -7.40576
O -6.89973 -7.26167 -7.14846
O -7.08043 -7.42371 0.86842
O 1.19181 0.89661 5.05697

O -7.03059 -7.30659 -3.21362
O 1.20203 0.89175 -3.29291
O 3.23079 -7.43296 2.96087
O -5.03986 0.89870 -5.34818
O -5.05960 0.88036 2.99051
O 3.28495 0.89515 3.01622
O 3.29123 0.88321 -5.38037
O -7.02527 -7.31214 4.91131
O 1.17599 -7.41558 -3.23125
O 1.17356 -7.45459 5.00662
O -7.15077 0.88482 -3.25420
O -2.97811 -1.17345 -5.43657
O 5.33776 5.09560 -3.26004
O -4.94959 -7.43380 2.94715
O 5.38056 -1.18480 -5.40372
O 7.53358 0.88887 2.95171
O -4.99659 -7.38889 -5.29405
O 7.50062 0.88463 -5.25930
O -0.89672 0.88906 2.97504
O -0.90216 0.89456 -5.41164
O 7.37021 -7.36598 2.90941
O -0.88134 -7.43652 2.98212
O -0.87687 -7.48106 -5.32701
O 7.38998 7.08360 4.89665
O 7.29491 7.10063 -3.19546
O -0.88402 7.17839 4.95415

O -0.88967 7.17006 -3.22815
O 7.51519 -1.17245 5.03735
O 7.42599 -1.17394 -3.27735
O -0.90026 -1.18796 5.07044
O -0.89424 -1.19059 -3.30615
O 7.31360 7.08846 0.87489
O 7.25405 6.87892 -7.25530
O -0.88237 7.13994 0.89195
O -0.87795 7.02754 -7.35849
O 7.47081 -1.19125 0.87595
O 7.35132 -1.17852 -7.38055
O -0.90246 -1.19889 0.89924
O -0.87725 -1.17800 -7.47375
O 5.30746 7.14738 2.93193
O 5.23319 7.13049 -5.22441
O -2.97090 7.15784 2.97110
O -2.93828 7.17639 -5.31226
O 5.30435 5.05991 5.05568
O 3.21556 7.15098 5.01334
O -7.18089 0.88264 4.96029
O 7.40044 2.92333 5.03142
O -7.22515 -3.25384 0.88661
O -7.16969 -5.25279 -5.20755
O 3.30847 2.97144 0.89904
O -0.90155 2.99239 -3.25291
O 7.46500 -5.22714 4.98065

O 7.43829 -5.26377 -3.22343
O -0.89628 -5.38248 5.09816
O -0.89272 -5.39742 -3.29549
O 7.50314 5.02001 2.93787
O 7.41463 4.91111 -5.25407
O -0.88504 5.08465 2.96622
O -0.88907 5.11541 -5.37797
O 7.50989 -3.23636 2.96444
O 7.51437 -3.20957 -5.24113
O -0.88514 2.95283 5.05576
O -0.89123 -3.31344 2.99330
O 5.36966 0.88889 0.89406
O 5.32160 0.88803 -7.40752
O -3.00071 0.89210 0.90650
O -2.98274 0.88384 -7.54102
O 5.28732 -7.41099 0.87350
O -2.93969 -7.46894 0.88050
O -2.95523 -7.31375 -7.34300
O 1.19339 2.96935 3.01491
O 1.18188 2.95788 -5.35875
O -7.14242 2.95629 2.95556
O -7.20060 2.93558 -5.26522
O 1.18868 -5.35363 2.95148
O -0.88112 -3.27036 -5.38015
O 1.18143 -5.33906 -5.40539
O -2.93112 -5.30879 7.23847

O 5.35533 -5.30133 -5.35587
O 7.49989 2.95010 -3.25034
O 7.50611 2.94315 0.88600
O 7.45230 -5.31903 0.87671
O -0.87506 2.95668 -7.45565
O -0.89137 2.99382 0.90270
O 7.38733 2.91483 -7.38421
O -7.06916 -5.25236 7.10289
O -7.10735 -5.29227 -1.18323
O -0.87491 -5.27191 -7.44917
O 1.18889 -5.38916 -1.19008
O 1.16791 -5.28877 7.24774
O -7.16885 2.98435 -1.18930
O -2.94381 -5.37371 2.96757
O -7.11507 2.90874 7.09699
O -2.97076 2.96613 7.24227
O 5.24037 2.94680 7.20169
O 5.41347 2.94919 -1.18621
O -3.00697 2.97606 -1.19139
O 5.26112 -5.29184 7.07737
O 5.41391 -5.36412 -1.19791
O 1.18580 3.01916 -1.19986
O -2.96651 -5.37448 -1.19261
O 5.39011 2.96032 2.94722
O 5.37149 2.92610 -5.37131
O -2.96514 2.97399 2.99281

O -2.96848 2.99769 -5.39569
O 5.37271 -5.37925 2.92258
O -0.89948 -5.36361 0.88923
O -7.11337 -5.33244 2.95491
O 1.17977 2.98266 7.15416
O -7.06736 -3.23873 -7.36752
O -5.14509 2.96099 0.88334
O 1.17916 5.08913 5.06810
O -4.97335 2.94306 -7.41511
O 3.29301 -5.40831 0.88384
O 3.21569 -5.25694 -7.53878
O -5.05769 -5.39248 0.88504
O -4.94497 -5.25968 -7.48384
O 7.37316 4.89603 7.09407
O 7.40277 5.04708 -1.18537
O -0.87886 4.97685 7.14650
O -0.89250 5.12182 -1.18846
O 7.33700 -3.21588 7.03919
O -0.87619 -3.25126 7.21597
O -0.90181 -3.30568 -1.19554
O 1.18527 5.13664 -3.26067
O 3.21555 4.95209 7.22372
O -7.16914 4.94679 4.96087
O -7.22918 4.94526 -3.25446
O 1.19368 -3.25184 5.07121
O 1.19703 -3.26034 -3.31526

O -7.10691 -3.24724 5.00985
O -7.17586 -3.24233 -3.22173
O 1.19936 5.09619 0.90030
O 1.18158 4.97830 -7.46499
O -7.16971 4.95511 0.87916
O -7.05256 4.94928 -7.33032
O 1.20269 -3.26328 0.90458
O -2.97351 -5.38345 -5.40506
O 1.18534 -3.25291 -7.42321
O 3.27333 5.13262 -1.19608
O -5.03093 5.02262 -1.18486
O 7.49038 -3.26704 -1.17027
O 3.27526 2.97239 -3.27786
O 3.25649 2.93852 -7.49877
O -2.93052 -3.26553 -7.54231
O 3.21967 -3.23624 7.13580
O 3.31236 -3.29405 -1.18221
O -4.96906 -3.20066 7.20428
O -5.06560 -3.29476 -1.19153
O 3.24992 5.07487 2.95608
O 3.23509 5.07951 -5.39450
O -5.07165 5.07456 2.92303
O 3.28316 -3.31076 2.98061
O 3.25906 -3.27802 -5.37868
O -5.11818 -3.26589 3.00091
O -5.06786 -3.25386 -5.34788

O 3.26545 2.94727 5.06624
O -5.08899 5.06677 -5.35530
O -4.94090 4.97779 7.11461
O -2.96622 -3.29395 0.90443
O -5.07620 2.95118 5.01686
O 5.37398 -3.29591 0.88480
O -2.93291 5.00581 -7.46720
O -2.96018 5.14581 0.88361
O 5.22735 4.98059 -7.36531
O 5.36607 5.02396 0.89256
O 5.31713 -3.21011 -7.41077
O -5.03153 -5.34870 5.04570
O 3.25699 -5.33023 -3.26596
O 3.22459 -5.36943 5.05340
O -5.09404 2.94395 -3.24920
O -5.03912 -5.34075 -3.27411
Ni -5.06191 -7.42874 0.88505
Ni -4.96246 -7.32621 -7.21226
Ni 7.48211 5.05730 0.88749
Ni 7.20933 4.91607 -7.23206
Ni -0.89660 5.14179 0.88930
Ni 7.49304 -3.25044 0.88287
Ni -0.89334 -3.32377 0.89558
Ni 5.38905 0.89035 -5.40835
Ni -5.05392 0.89302 0.89226
Ni 3.24889 -7.45691 0.88975

Ni -0.88149 5.06360 -7.43565
Ni -5.04410 0.87561 -7.40181
Ni 5.39800 -5.37738 -3.25407
Ni -2.98055 2.96856 -3.27798
Ni 3.29004 0.90187 0.89863
Ni -0.89020 -7.52764 -3.25088
Ni -0.87347 -7.51124 5.03803
Ni 7.25419 -7.19880 4.91912
Ni -0.89411 0.90059 -3.29012
Ni -0.89411 0.89250 5.13183
Ni 7.54605 0.89365 -3.28079
Ni 7.44550 0.87344 5.05109
Ni -2.98701 -5.36381 -3.23234
Ni -2.98483 -5.34035 5.06502
Ni -2.99581 2.99140 5.09797
Ni 3.21740 0.89416 -7.43007
Ni 5.35424 2.98542 -3.29421
Ni 5.33941 5.09775 -1.18751
Ni -2.99378 5.10420 -1.18531
Ni 5.26472 -5.33007 5.04031
Ni -7.00836 -7.27114 -1.18280
Ni -6.81346 -7.01624 6.70600
Ni 1.19122 -7.44732 -1.18228
Ni 1.17655 -7.38315 7.05715
Ni -7.20158 0.88015 -1.17364
Ni -7.05710 0.87915 7.01343

Ni 1.19149 0.89727 -1.18305
Ni 1.18086 0.88283 7.13795
Ni -2.93910 -1.19176 -7.47742
Ni -3.01219 -1.19495 0.90450
Ni 5.31881 -1.16515 -7.46919
Ni 5.42483 -1.19757 0.88796
Ni -2.88896 7.01637 -7.25464
Ni -2.95373 7.23158 0.88693
Ni 5.23547 7.02923 -7.23534
Ni 5.29938 7.21059 0.87976
Ni -6.91509 -5.21466 -7.26797
Ni -7.18199 -5.31282 0.87224
Ni 1.17527 -5.33106 -7.39806
Ni 1.17909 -5.40131 0.89284
Ni -7.04793 2.87149 -7.36963
Ni -7.23767 2.94592 0.88507
Ni 1.17313 2.97478 -7.41327
Ni 1.19007 2.96730 0.90274
Ni -3.01090 -3.27331 -1.19374
Ni -2.95267 -3.23838 7.16294
Ni 5.38485 -3.25164 -1.19482
Ni 5.30700 -3.20212 7.16106
Ni 5.30784 2.95564 5.02877
Ni -2.92096 4.99001 7.16111
Ni -5.02289 -3.25259 5.09547
Ni 5.30979 5.02207 7.13745

Ni -0.87803 2.93153 7.15818
Ni 1.17659 -3.27522 -5.39711
Ni 1.18950 -3.30665 2.99378
Ni -7.13965 4.94671 -5.24177
Ni -7.22580 4.96556 2.93191
Ni 1.17296 5.04359 -5.34243
Ni 1.18353 5.12877 2.94928
Ni -7.16261 -1.17877 -3.25892
Ni -7.15772 -1.16706 5.03242
Ni 1.19652 -1.19929 -3.28423
Ni 1.18975 -1.17874 5.15442
Ni -7.05042 6.99911 -3.21256
Ni -6.98872 6.97589 4.96537
Ni 1.17728 7.10378 5.05058
Ni 1.17292 7.18359 -3.23489
Ni -5.05243 -3.28898 -3.26933
Ni 3.27038 5.09927 5.01169
Ni -0.89805 3.00808 -1.19804
Ni 7.24219 -5.24976 6.96187
Ni 7.45729 -5.33394 -1.17174
Ni -0.87482 -5.37016 7.23712
Ni -0.88267 -5.40306 -1.19253
Ni -7.20773 -3.25371 -5.26273
Ni 3.24537 5.12852 -3.24059
Ni -5.04087 5.09703 -3.26959
Ni 3.25421 -3.27832 5.12354

Ni 3.30797 -3.28336 -3.28088
Ni -5.05341 5.03234 5.05125
Ni -7.16301 -3.25562 2.93445
Ni 7.52734 2.97968 -1.17968
Ni -5.10655 2.96919 2.98485
Ni -0.89503 -1.19540 -5.42994
Ni 3.25369 2.97265 2.99981
Ni -0.89753 -1.18214 2.97400
Ni 7.42261 -1.17197 -5.27800
Ni 7.47441 -1.18732 2.94244
Ni -0.87119 7.21130 -5.33237
Ni -0.89038 7.15130 2.95349

Ni 7.24821 7.02587 -5.21301
Ni 7.25600 7.03238 2.90446
Ni -4.99053 -5.32736 -5.31327
Ni -5.05878 -5.36454 2.96650
Ni 3.27236 -5.39980 -5.31701
Ni 3.23397 -5.41803 2.95621
Ni -5.01253 2.96161 -5.34768
Ni 3.25556 2.96210 -5.35175
Ni -5.09988 -1.17528 -1.17886
Ni 7.25402 2.91102 7.06376
Ni -5.04112 -1.18363 7.15959
Ni 3.28474 -1.18449 -1.18939

Ni 3.25448 -1.17305 7.16991
Ni -5.02316 7.22985 -1.17469
Ni -4.95577 6.92149 6.97516
Ni 3.21961 7.20637 -1.18058
Ni 3.18794 6.99258 6.96668
Ni -2.95599 -7.43870 -5.26605
Ni -2.94647 -7.52594 2.93019
Ni 5.28824 -7.49550 2.95956
Ni -2.96515 0.88262 -5.42585
Ni -3.01006 0.89180 3.00643
Ni -0.88225 -3.24849 -7.50233
Ni 5.42966 0.89202 2.96945

References

(S1) Alessi, B.; Macias-Montero, M.; Maddi, C.; Maguire, P.; Svrcek, V.; Mariotti, D. Bridging energy bands to the crystalline and amorphous states of Si QDs. *Faraday Discuss.* **2020**, *222*, 390–404.

(S2) TURBOMOLE 7.2, TURBOMOLE GmbH Karlsruhe, http://www.turbomole.com. TURBOMOLE is a development of University of Karlsruhe and Forschungszentrum Karlsruhe 1989-2007, TURBOMOLE GmbH since 2007.

(S3) Yanai, T.; Tew, D. P.; Handy, N. C. A new hybrid exchange–correlation functional using the Coulomb-attenuating method (CAM-B3LYP). *Chem. Phys. Lett.* **2004**, *393*, 51–57.

(S4) Plessow, P.; Weigend, F. Seminumerical calculation of the Hartree–Fock exchange

matrix: Application to two-component procedures and efficient evaluation of local hybrid density functionals. *J. Comput. Chem.* **2012**, *33*, 810–816.

(S5) Weigend, F.; Ahlrichs, R. Balanced basis sets of split valence, triple zeta valence and quadruple zeta valence quality for H to Rn: Design and assessment of accuracy. *Phys. Chem. Chem. Phys.* **2005**, *7*, 3297.

(S6) Weigend, F. Accurate Coulomb-fitting basis sets for H to Rn. *Phys. Chem. Chem. Phys.* **2006**, *8*, 1057.

(S7) Perdew, J. P.; Burke, K.; Ernzerhof, M. Generalized Gradient Approximation Made Simple. *Phys. Rev. Lett.* **1996**, *77*, 3865–3868.

(S8) Perdew, J. P.; Burke, K.; Ernzerhof, M. Generalized Gradient Approximation Made Simple [Phys. Rev. Lett. 77, 3865 (1996)]. *Phys. Rev. Lett.* **1997**, *78*, 1396–1396.

(S9) Heyd, J.; Scuseria, G. E.; Ernzerhof, M. Hybrid functionals based on a screened Coulomb potential. *J. Chem. Phys.* **2003**, *118*, 8207–8215.

(S10) Heyd, J.; Scuseria, G. E.; Ernzerhof, M. Erratum: "Hybrid functionals based on a screened Coulomb potential" [J. Chem. Phys. 118, 8207 (2003)]. *J. Chem. Phys.* **2006**, *124*.

(S11) Krukau, A. V.; Vydrov, O. A.; Izmaylov, A. F.; Scuseria, G. E. Influence of the exchange screening parameter on the performance of screened hybrid functionals. *J. Chem. Phys.* **2006**, *125*.

(S12) Adamo, C.; Barone, V. Toward reliable density functional methods without adjustable parameters: The PBE0 model. *J. Chem. Phys.* **1999**, *110*, 6158–6170.

(S13) Ernzerhof, M.; Scuseria, G. E. Assessment of the Perdew–Burke–Ernzerhof exchange-correlation functional. *J. Chem. Phys.* **1999**, *110*, 5029–5036.

(S14) Li, M.; Reimers, J. R.; Ford, M. J.; Kobayashi, R.; Amos, R. D. Accurate prediction of the properties of materials using the <scp>CAM-B3LYP</scp> density functional. *J. Comput. Chem.* **2021**, *42*, 1486–1497.